NASA TECHNICAL NOTE

NASA TN D-5425

NASA TN D-5425

NUMERICAL INTEGRATION IN A RIGID-BODY TRAJECTORY PROGRAM

by John Edd Moore

George C. Marshall Space Flight Center
Marshall, Ala.

NATIONAL AERONAUTICS AND SPACE ADMINISTRATION • WASHINGTON, D. C. • SEPTEMBER 1969

1. REPORT NO.	2. GOVERNMENT ACCESSION NO.	3. RECIPIENT'S CATALOG NO.
NASA TN D-5425		

4. TITLE AND SUBTITLE

NUMERICAL INTEGRATION IN A RIGID-BODY TRAJECTORY PROGRAM

5. REPORT DATE: September 1969

6. PERFORMING ORGANIZATION CODE

7. AUTHOR(S)

John Edd Moore

8. PERFORMING ORGANIZATION REPORT #: M153

9. PERFORMING ORGANIZATION NAME AND ADDRESS

Aero-Astrodynamics Laboratory
Marshall Space Flight Center, Alabama 35812

10. WORK UNIT NO.

11. CONTRACT OR GRANT NO.

13. TYPE OF REPORT & PERIOD COVERED: TECHNICAL NOTE

12. SPONSORING AGENCY NAME AND ADDRESS

National Aeronautics and Space Administration
Washington, D.C. 20546

14. SPONSORING AGENCY CODE

15. SUPPLEMENTARY NOTES

This work was submitted to the Graduate School of Vanderbilt University, Nashville, Tennessee, in partial fulfillment of the requirements for the degree of Master of Science.

16. ABSTRACT

This report compares the fourth-order Runge-Kutta numerical integration technique with two of Dr. E. B. Shanks' numerical integration formulas in a mathematical model used for computing rigid body, first-stage trajectories of a Saturn space vehicle. The scope of the problem is to describe the mathematical model and to present a derivation of the differential equations of motion which it comprises; to establish a basis for comparing the integration techniques; and to generate sufficient comparison data to establish which integration technique is the most practical to use in this model from a standpoint of computer run time and accuracy.

As an employee of the National Aeronautics and Space Administration, the author was required to develop a computer program for simulating the first-stage flight of a Saturn space vehicle. The resulting program requires that six first-order and three second-order differential equations be numerically solved to predict the translational and rotational motion of a space vehicle. An efficient integration technique had to be chosen that would provide a solution within the accuracy of the data which describe the vehicle dynamic response characteristics. In a search for the most acceptable integration technique, the fourth-order Runge-Kutta formula and two of Dr. E. B. Shanks' integration formulas were each used in the program to compute the first-stage trajectory of a typical Saturn vehicle. Comparative data were generated for each formula over a range of integration step sizes. An analysis of the data showed a fourth-order formula developed by Dr. Shanks to be the most practical integration technique to use in computer programs of this type from a standpoint of computation time, accuracy, and stability of the solution.

17. KEY WORDS	18. DISTRIBUTION STATEMENT
	Unclassified - Unlimited

19. SECURITY CLASSIF. (of this report)	20. SECURITY CLASSIF. (of this page)	21. NO. OF PAGES	22. PRICE*
U	U	104	$3.00

*For sale by the Clearinghouse for Federal Scientific and Technical Information
Springfield, Virginia 22151

ACKNOWLEDGEMENTS

The author wishes to express his appreciation to Professor E. B. Shanks and Professor J. R. Wesson of the Vanderbilt University Department of Mathematics for their suggestions and encouragement during the preparation of this thesis. Also, three people in the Aero-Astrodynamics Laboratory at Marshall Space Flight Center deserve special thanks. Appreciation is extended to Mr. C. R. Fulmer for a technical review of the paper and to Mrs. Sarah Hightower for technically editing the paper. A debt is owed to Mrs. Evelyn Carter for an excellent job in preparing the final copies of the illustrations in the paper.

TABLE OF CONTENTS

LIST OF TABLES

LIST OF ILLUSTRATIONS

INTRODUCTION

The purpose of this thesis is to compare the fourth-order Runge-Kutta numerical integration technique with two of Dr. E. B. Shanks' numerical integration formulas in a mathematical model used for computing rigid body, first-stage trajectories of a Saturn space vehicle. The scope of the problem is to describe the mathematical model and to present a derivation of the differential equations of motion which it comprises; to establish a basis for comparing the integration techniques; and to generate sufficient comparison data to establish which integration technique is the most practical to use in this model from a standpoint of computer run time and accuracy.

As an employee of the National Aeronautics and Space Administration, the author was required to develop a computer program for simulating the first-stage flight of a Saturn space vehicle. The resulting program requires that six first-order and three second-order differential equations be numerically solved to predict the translational and rotational motion of a space vehicle. An efficient integration technique had to be chosen that would provide a solution within the accuracy of the data which describe the vehicle dynamic response characteristics. In a search for the most acceptable integration technique, the fourth-order Runge-Kutta formula and two of Dr. E. B. Shanks'

integration formulas were each used in the program to compute the first-stage trajectory of a typical Saturn vehicle. Comparative data were generated for each formula over a range of integration step sizes. These data are analyzed in Chapter V.

The first four chapters define the mathematical model in which the integration formulas are compared. This model consists of several smaller models that simulate the vehicle subsystems and the physical properties of the earth. These subsystems and the earth's physical characteristics are described in Chapter I. The different coordinate systems to which the model refers motion and the related transformations are defined in Chapter II, and the differential equations of motion are derived in Chapter III. In Chapter IV, a definition of the mathematical model is completed with a description of the forces and moments that act upon a space vehicle during flight.

CHAPTER I

SATURN VEHICLE SUBSYSTEMS AND PHYSICAL PROPERTIES OF THE EARTH TO BE SIMULATED

In order to design and build an extremely complex and expensive vehicle such as the Saturn V, a means of simulating or predicting how a space vehicle with specific subsystems and dynamic characteristics will react during actual flight is mandatory. To this end, mathematical models are developed for each subsystem and then combined into a total model of the vehicle. Models of the earth's shape, gravity field, and atmosphere are merged with the vehicle model to establish a two-body system. The total model is then programmed on an electronic computer and used for predicting the response of a vehicle to various atmospheric conditions and vehicle tolerances.

The Saturn V subsystems that guide and control the vehicle will be described first. A knowledge of these subsystems and their functions is necessary before a model can be developed to simulate them.

In this paper the terms navigation, guidance, and control are defined as follows:

Navigation is the determination of the vehicle's present position and velocity from measurements made onboard the vehicle.

Guidance is the computations of maneuvers necessary to achieve the desired flight path.

Control is the execution of the guidance maneuver by controlling the direction of part of the vehicle's thrust.

The Saturn V launch vehicle is guided during powered flight by navigation, guidance, and control equipment located in the Instrument Unit (IU). An inertial platform is used to provide three orthogonal space-stabilized directions for acceleration and attitude measurements. A launch vehicle digital computer (LVDC) solves guidance equations, and an analog flight control computer executes flight control functions. Analog signals are converted to digital numbers and vice versa by means of a launch vehicle data adapter (LVDA).

The vehicle-fixed coordinate system and the Saturn sign convention for control variables are presented in Figure 1. Rotational motion about the X_m axis is called roll motion, rotational motion about the Y_m axis is called pitch motion, and rotational motion about the Z_m axis is referred to as yaw motion.

Figure 2 presents the Saturn V inertial platform configuration. The gimbal system allows the vehicle to rotate freely without disturbing the gyro-stabilized inertial gimbal. An orthogonal, right-handed, space-fixed coordinate system (X, Y, Z) is established by the input axes of three single-degree-of-freedom gyroscopes. Acceleration and attitude measurements are taken with respect to this coordinate system. Three integrating accelerometers, mounted on the platform's inertial gimbal, measure the three components of

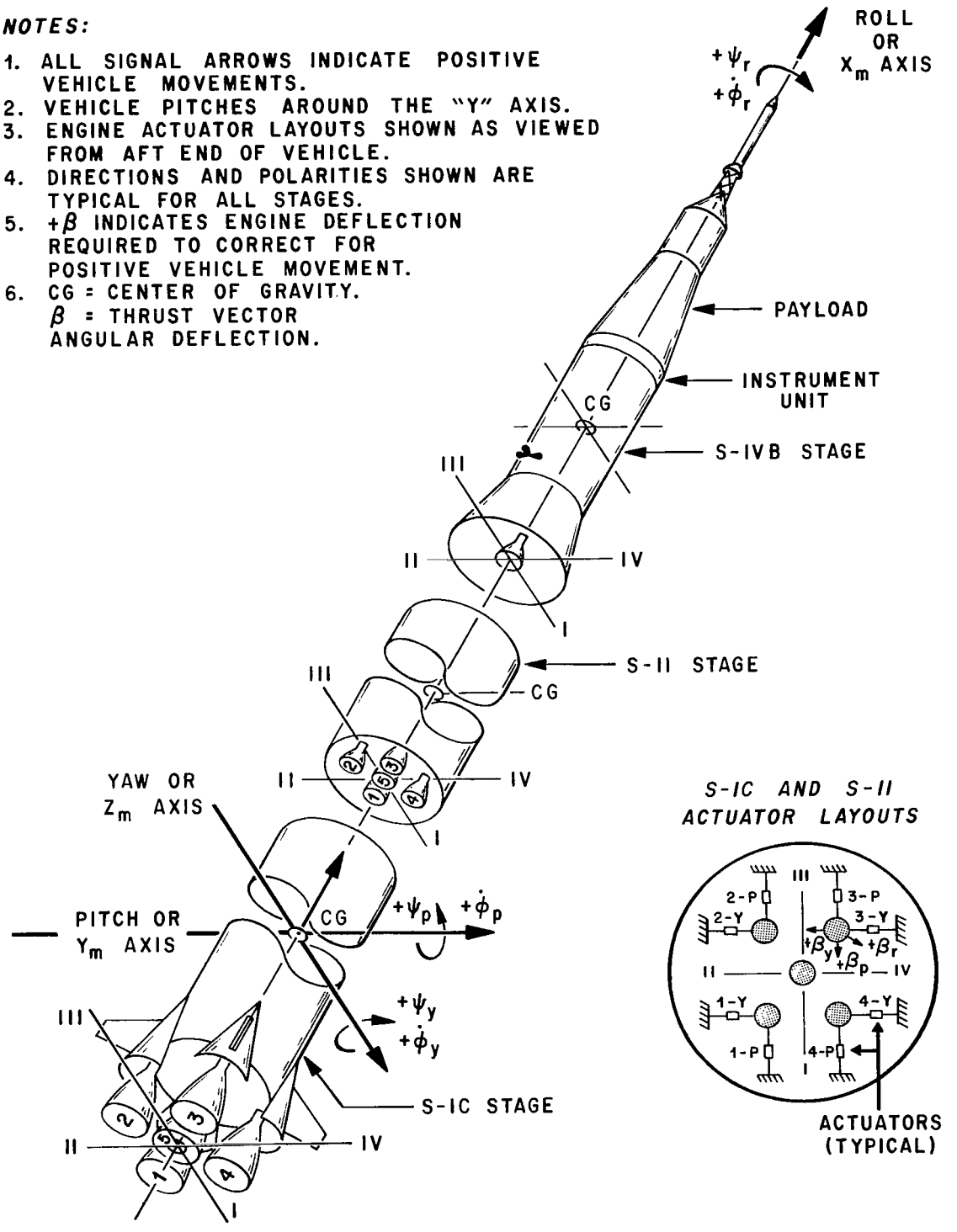

FIG. 1. SATURN V VEHICLE CONFIGURATION AND SIGN CONVENTION

NOTE:

IA = INPUT AXIS

OA = OUTPUT AXIS

SRA = SPIN REFERENCE AXIS

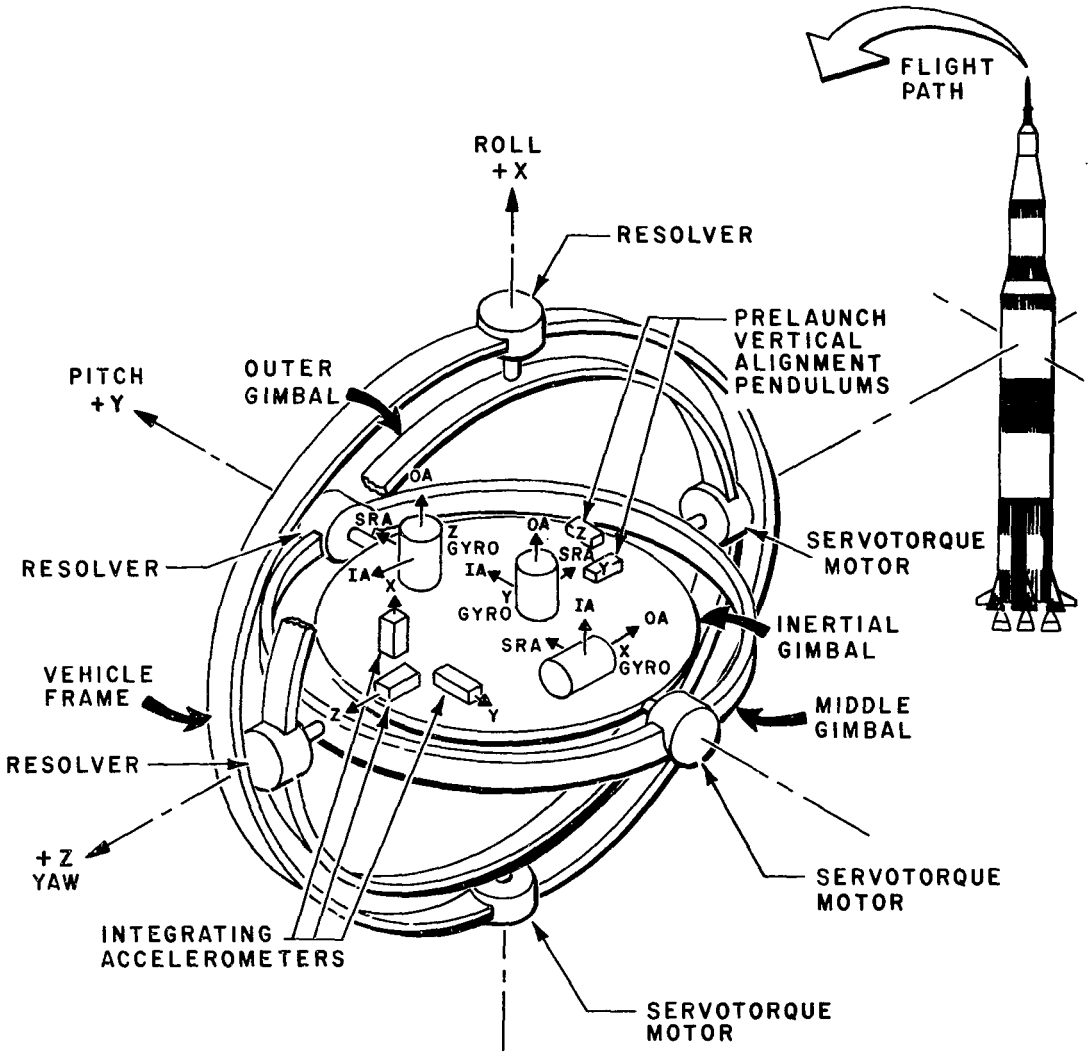

FIG. 2. THE SATURN V INERTIAL PLATFORM GIMBAL CONFIGURATION

velocity. Vehicle attitude is measured by resolvers located at the gimbal pivot points.

The three angles measured by the inertial platform resolvers are classically known as Eulerian angles, a discussion of which should aid in understanding the function of the platform.

Eulerian angles evolved from the problem of describing the orientation of a rigid body that is free to turn about a point 0. One solution would be to assign the coordinates of two particles in the body, not on the same line through 0. Because this method involves the use of six parameters that cannot be varied independently, it is rejected. A much simpler method is to define the orientation of the body with respect to a reference frame by the use of three Eulerian angles.

Figure 3 shows two orthogonal right-handed triads (X, Y, Z) and (X_m, Y_m, Z_m) with their origins at point 0. The triad (X_m, Y_m, Z_m) is fixed in a rigid body that is free to turn about 0, and the triad (X, Y, Z) serves as a frame of reference. Assuming that the (X_m, Y_m, Z_m) triad initially coincides with the reference triad, it can be revolved to the orientation shows in Figure 3 by the three following right-hand rotations.

1. First rotate about Y through φ_p. This brings the movable triad (X_m, Y_m, Z_m) into coincidence with (X', Y, Z').

2. Next, rotate about Z' through φ_y. This brings (X_m, Y_m, Z_m) into coincidence with (X_m, Y', Z').

3. Finally, rotate about X_m through φ_r. This brings (X_m, Y_m, Z_m) into the final position.

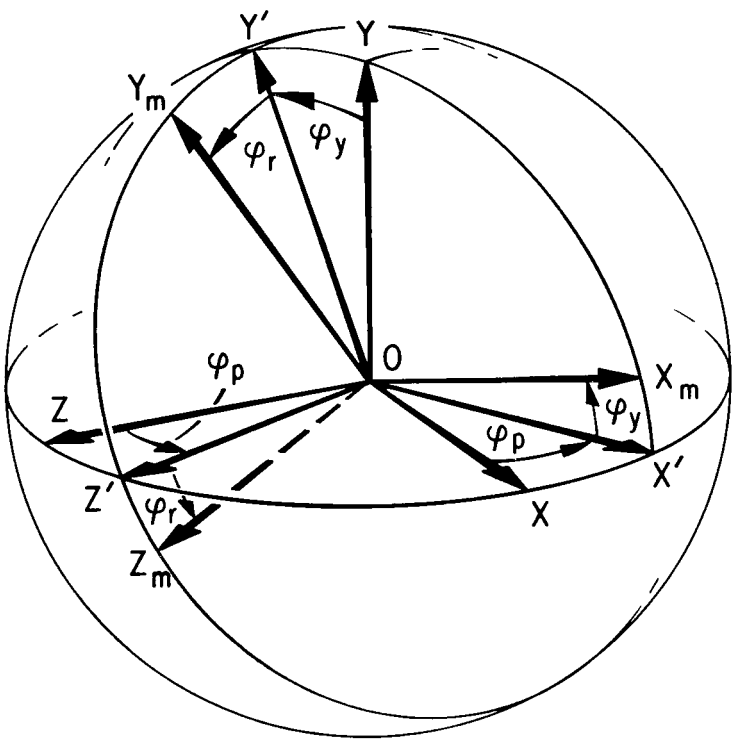

FIG. 3. EULERIAN ANGLES

Note that all possible positions of the body can be obtained by assigning values to φ_p, φ_y, and φ_r in the ranges $0 \leq \varphi_p < 2\pi$, $0 \leq \varphi_y \leq \pi$, and $0 \leq \varphi_r \leq 2\pi$.

The symbols used in the discussion of Eulerian angles were chosen to coincide with those used in Figures 1 and 2. That is, the (X, Y, Z) triad is the one established by the vehicle inertial platform and the (X_m, Y_m, Z_m) triad corresponds to the vehicle-fixed triad in Figure 1. An inspection of Figure 2 reveals that the Eulerian angles φ_p, φ_y, φ_r are precisely the angles measured by the inertial platform resolvers.

Attitude control is achieved during the S-IC stage of powered flight by gimbaling or deflecting the stage's four outboard engines (engines 1 through 4 in Figure 1). Each of these four engines has two hydraulic actuators for gimbaling the engine about its stage attach point. To determine the amount these engines are to be gimbaled, the LVDC compares the instantaneous vehicle attitude with the attitude computed by the guidance scheme. Attitude error signals (ψ_p, ψ_y, ψ_r) are derived from the difference between the platform gimbal angles $(\varphi_p, \varphi_y, \varphi_r)$ and the desired attitude angles (χ_p, χ_y, χ_r). The vehicle angular velocities about the X_m, Y_m, and Z_m axes are measured by three rate gyroscopes located in the IU. In the flight control computer, the signals from the rate gyroscopes $(\dot{\phi}_p, \dot{\phi}_y, \dot{\phi}_r)$ and the attitude error signals are filtered, multiplied by a gain factor, and then combined to generate the control commands for the engine actuators. The attitude error equations and the control laws for combining the filtered attitude errors and vehicle angular rates are presented in Chapter IV.

During the S-IC stage of flight, the vehicle must execute pitch, yaw, and roll maneuvers. A yaw maneuver during the first critical seconds of flight guides the vehicle away from the launch umbilical tower. The Z_m axis is aligned along the flight azimuth by the roll maneuver. The pitch maneuver is designed to guide the vehicle along a flight path that results in minimum aerodynamic structural loading. This maneuver allows the vehicle to build a component of velocity tangent to the earth's surface as it gains altitude. All three maneuvers are preprogrammed in the LVDC as time-dependent polynomials.

The LVDC contains a closed-loop guidance scheme for providing guidance commands during the S-II and S-IVB stages of powered flight. This scheme determines attitude commands from the components of position and velocity of the vehicle center of gravity (CG) relative to a space-fixed coordinate system orientated as the (X, Y, Z) platform coordinate system. Initial velocity of the vehicle because of the earth's rotation and the platform velocity from the integrating accelerometers are algebraically summed by the LVDC to obtain space-fixed velocity of the vehicle. Position is determined by integrating the space-fixed vehicle velocity.

With the description of the major vehicle subsystems complete, a presentation of the models of the earth's shape, motion, gravity field, and atmosphere can now be given. The standard model for the earth's shape is known as the Fischer Ellipsoid, a model which considers the earth to be an elliptical spheroid (Figure 4). The intersection of the earth and a plane that

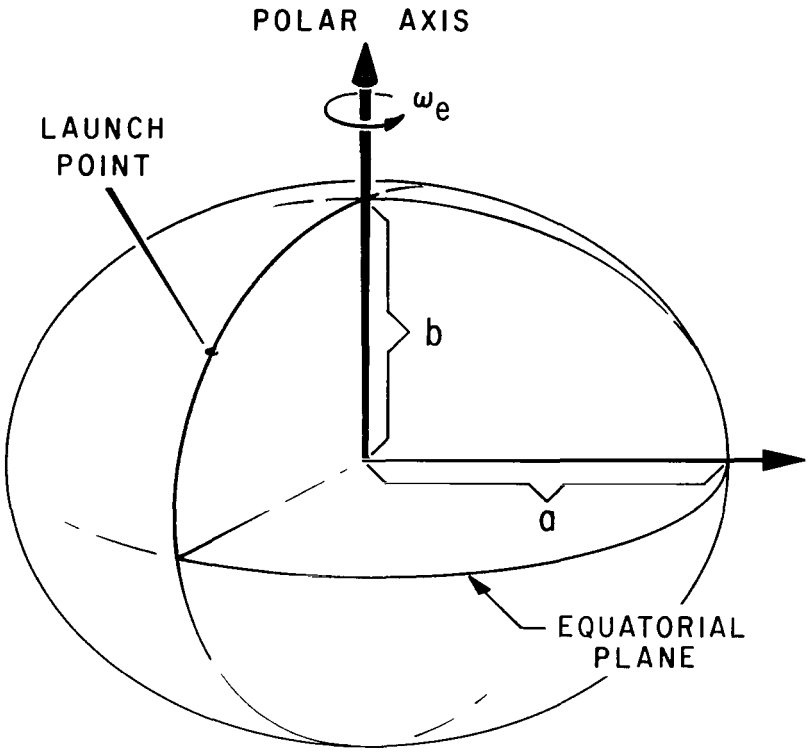

a EQUATORIAL RADIUS OF EARTH

b POLAR RADIUS OF EARTH

ω_e MAGNITUDE OF EARTH'S ROTATIONAL VELOCITY

FIG. 4. THE FISCHER ELLIPSOID

contains the earth's polar axis is an ellipse; the intersection of the earth and a plane that is perpendicular to the polar axis is a circle.

The only motion of the earth that will be considered is rotational; that is, the center of the earth will be assumed fixed in space with the earth rotating about its polar axis. Translation of the earth about the sun and precession of the earth's polar axis during the year have no significant effect on the motion of a space vehicle with respect to the earth.

A Newtonian potential function is used to predict the magnitude and direction of the earth's gravity at any point above the earth's surface. The oblate potential of the earth is assumed to contain the second, third, and fourth spherical harmonics. A discussion of this potential is lengthy and will not be presented here. A complete treatment of the subject is given in Chapters I and II of Reference 1.

A model reference atmosphere for Cape Kennedy, Florida (Reference 2), which provides atmospheric information, is based on annual median values of measured atmospheric parameters. Multisegment polynomials define each atmospheric parameter as a function of altitude.

CHAPTER II

REFERENCE COORDINATE SYSTEMS AND TRANSFORMATIONS

In order to determine the motion of a vehicle with respect to the rotating earth, six reference three-dimensional coordinate systems are used. Each system is defined to be right-handed and orthogonal to simplify computation. Rotational motion of a vehicle is computed in the vehicle coordinate system (X_m, Y_m, Z_m) defined in Figure 2. The other five systems consist of two earth-fixed and three space-fixed systems. Here, the terms "space-fixed" and "earth-fixed" refer to coordinate systems that have constant orientation and position with respect to the solar system and the earth, respectively. The three space-fixed systems (Figure 5) are referred to as the surface triad (X_s, Y_s, Z_s), the earth-centered triad (X_c, Y_c, Z_c), and the equatorial triad (U, V, W). The two earth-fixed systems (Figure 6) are referred to as the launch-point triad (X_e, Y_e, Z_e) and the earth-equatorial triad (U_e, V_e, W_e).

At the instant the vehicle inertial platform is released, the origin of the (X_s, Y_s, Z_s) triad is located at the launch point. As time passes, the surface of the earth moves beneath the (X_s, Y_s, Z_s) origin because of the

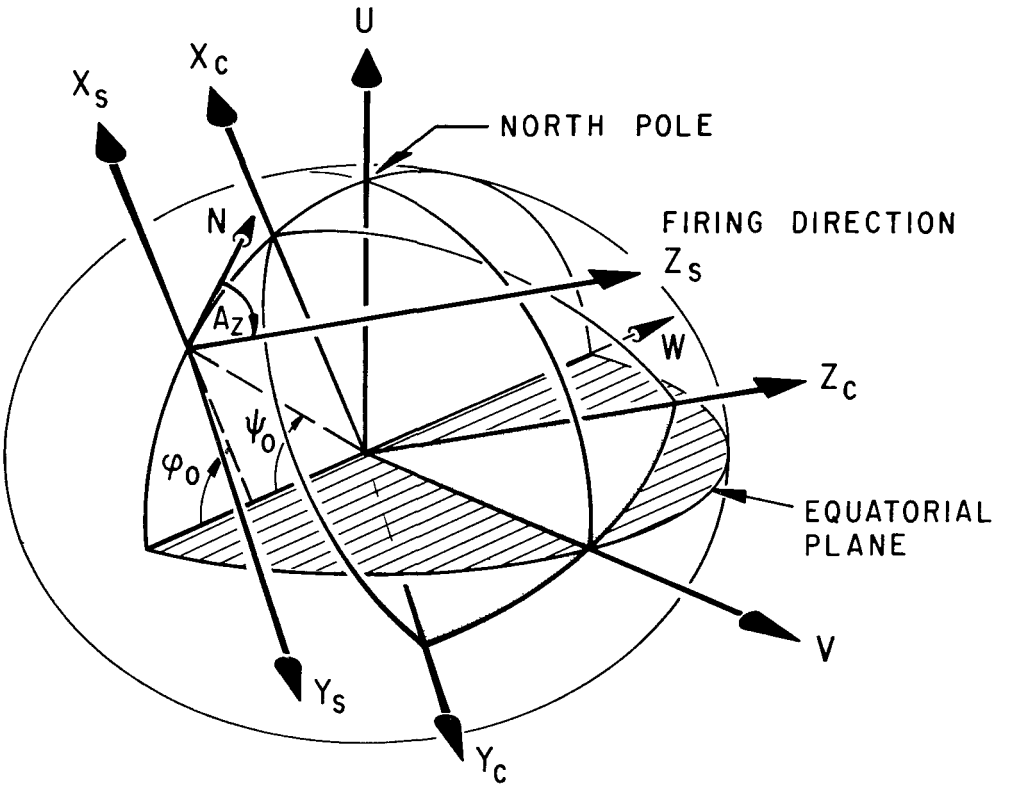

A_Z LAUNCH AZIMUTH

ψ_o GEOCENTRIC LATITUDE OF LAUNCH POINT

φ_o GEODETIC LATITUDE OF LAUNCH POINT

FIG. 5. SPACE-FIXED COORDINATE SYSTEMS

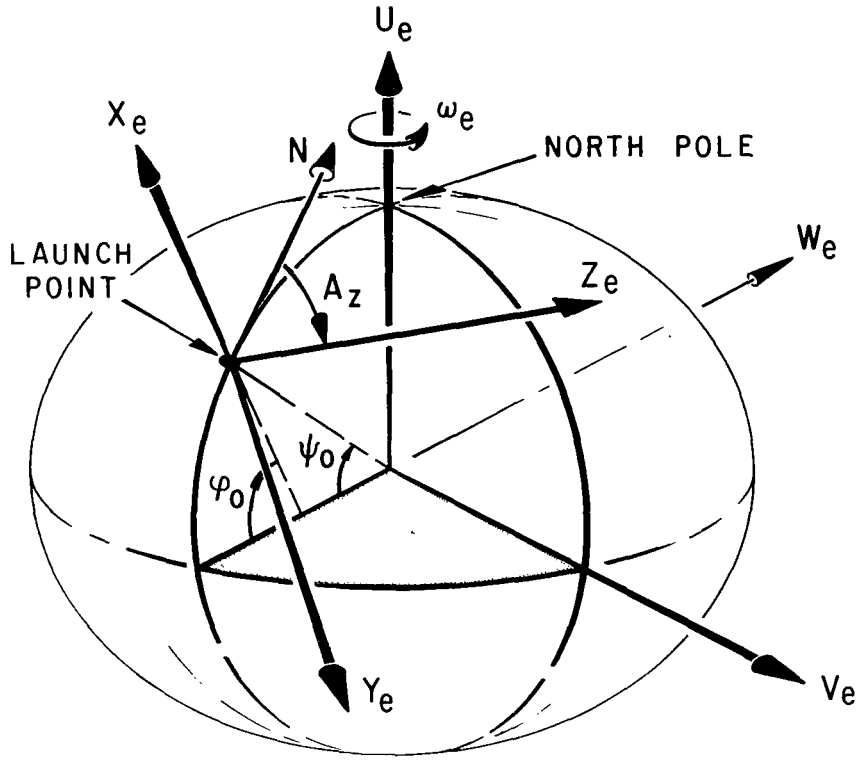

A_z LAUNCH AZIMUTH

ω_e MAGNITUDE OF EARTH'S ROTATIONAL VELOCITY

ψ_o GEOCENTRIC LATITUDE OF LAUNCH POINT

φ_o GEODETIC LATITUDE OF LAUNCH POINT

FIG. 6. EARTH-FIXED COORDINATE SYSTEMS

earth's rotation. This system is defined to have the same orientation as the (X, Y, Z) space-fixed triad established by the inertial platform (Figure 2). At release, the inertial platform X axis is aligned to the local vertical; the Z axis is tangent to the earth's surface at the launch site and lies in the flight plane; and the Y axis forms a right-hand system. The (X_s, Y_s, Z_s) triad is defined in this manner to simulate the function of the vehicle inertial platform.

The earth-centered triad (X_c, Y_c, Z_c) has the same orientation as the surface triad; its origin is located at the center of the earth as the name implies. Some of the initial conditions and certain trajectory parameters are computed with respect to this system.

A second earth-centered triad (U, V, W), the equatorial system, is defined to simplify computations that involve the earth's rotational velocity. The U axis, which is directed along the earth's rotational velocity vector, passes through the North Pole and is perpendicular to the equatorial plane. At the instant the vehicle inertial platform is released, the W axis lies in the plane of the launch meridian.

One earth-fixed triad (X_e, Y_e, Z_e) is used by the model for computing motion of the vehicle with respect to the launch point (Figure 6). This triad has its origin at the launch site and is coincident with the (X_s, Y_s, Z_s) triad at the instant the vehicle platform is released.

A second earth-fixed triad (U_e, V_e, W_e) has its origin at the center of the earth and is coincident with the (U, V, W) triad at platform release.

This system is used in deriving the transformation from the (X_s, Y_s, Z_s) system to the (X_e, Y_e, Z_e) system.

Since the objective of the total model is to determine the position and orientation of a vehicle at any time in flight in different coordinate systems, a procedure for transforming the coordinates of a vector from one triad to another is mandatory. This procedure can be established by developing a transformation between each pair of triads. A transformation is determined by the right-hand rotations required to carry the first triad to the same orientation as the second triad. Right-hand rotations are represented by 3×3 matrices.

Three basic right-hand rotations occur frequently throughout this paper. The transformations for these rotations follow:

$$[\theta]_x = \begin{bmatrix} 1 & 0 & 0 \\ 0 & \cos\theta & \sin\theta \\ 0 & -\sin\theta & \cos\theta \end{bmatrix}$$

$$[\theta]_y = \begin{bmatrix} \cos\theta & 0 & -\sin\theta \\ 0 & 1 & 0 \\ \sin\theta & 0 & \cos\theta \end{bmatrix}$$

$$[\theta]_z = \begin{bmatrix} \cos\theta & \sin\theta & 0 \\ -\sin\theta & \cos\theta & 0 \\ 0 & 0 & 1 \end{bmatrix}$$

Here, $[\theta]_x$ is the transformation for a right-hand rotation about the X axis through an angle θ ; $[\theta]_y$ is the transformation for a right-hand rotation about the Y axis through an angle θ ; and $[\theta]_z$ is the transformation for a

right-hand rotation about the Z axis through an angle θ . An inspection of Figure 7 makes a derivation of these transformations trivial. All three transformation are orthogonal since $[\theta]_i^T [\theta]_i = [\theta]_i [\theta]_i^T = [I]$, for $i = x, y, z$ where $[I]$ is the identity matrix. Hence, the transpose equals the inverse. This fact will be used extensively throughout this paper. All of the transformations required by the model will be combinations of these three basic ones.

Two rotations are required to align the surface triad with the equatorial triad. A right-hand rotation about the X_s axis through the angle A_z will carry the Z_s axis into the launch meridian plane (Figure 5). Then a negative right-hand rotation about the new Y_s axis through the angle $\left(\frac{\pi}{2} - \varphi_o\right)$ will complete the alignment. Hence,

$$\bar{u} = \begin{bmatrix} u \\ v \\ w \end{bmatrix} = \left[\varphi_o - \frac{\pi}{2}\right]_y \left[A_z\right]_x \begin{bmatrix} x_s \\ y_s \\ z_s \end{bmatrix} = \left[\varphi_o - \frac{\pi}{2}\right]_y \left[A_z\right]_x \bar{x}_s \tag{2-1}$$

and

$$\bar{x}_s = \left[A_z\right]_x^T \left[\varphi_o - \frac{\pi}{2}\right]_y^T \bar{u} \quad . \tag{2-2}$$

Since the surface triad and the earth-centered triad have the same orientation, the above transformation will apply there also. This is

$$\bar{u} = \begin{bmatrix} u \\ v \\ w \end{bmatrix} = \left[\varphi_o - \frac{\pi}{2}\right]_y \left[A_z\right]_x \begin{bmatrix} x_c \\ y_c \\ z_c \end{bmatrix} = \left[\varphi_o - \frac{\pi}{2}\right]_y \left[A_z\right]_x \bar{x}_c \tag{2-3}$$

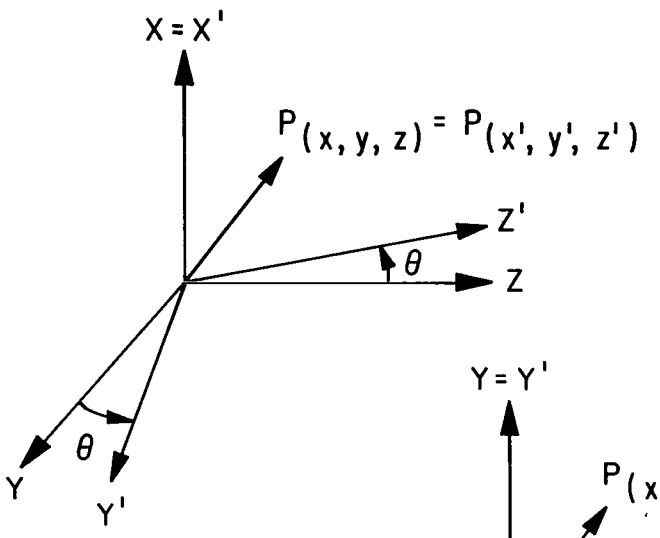

$$\begin{bmatrix} x' \\ y' \\ z' \end{bmatrix} = [\theta]_x \begin{bmatrix} x \\ y \\ z \end{bmatrix}$$

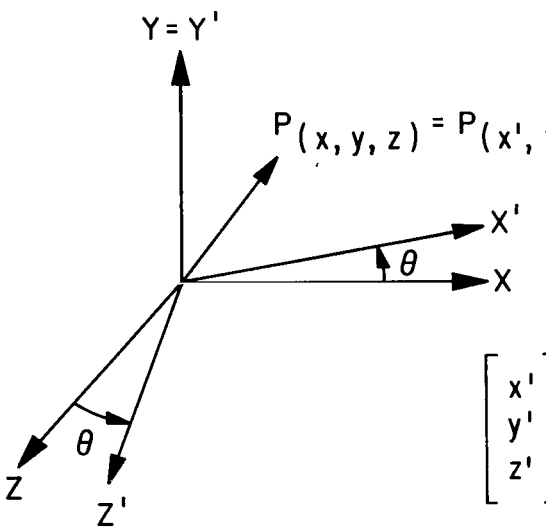

$$\begin{bmatrix} x' \\ y' \\ z' \end{bmatrix} = [\theta]_y \begin{bmatrix} x \\ y \\ z \end{bmatrix}$$

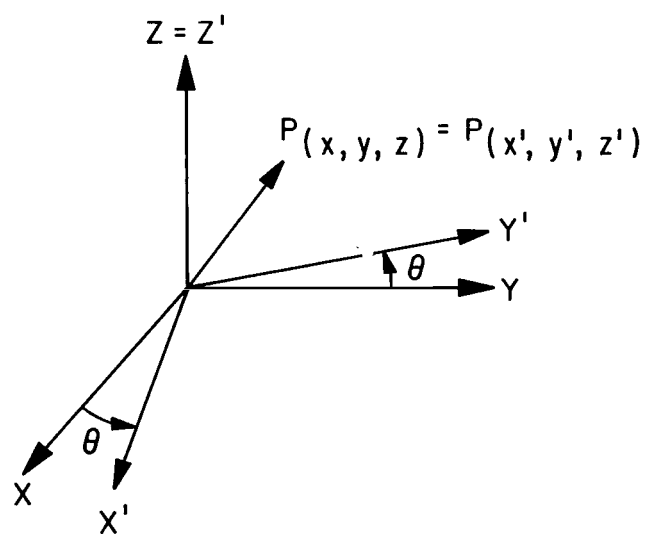

$$\begin{bmatrix} x' \\ y' \\ z' \end{bmatrix} = [\theta]_z \begin{bmatrix} x \\ y \\ z \end{bmatrix}$$

FIG. 7. TRANSFORMATIONS FOR RIGHT-HAND ROTATIONS

and

$$\overline{x}_c = \left[A_z\right]_x^T \left[\varphi_o - \frac{\pi}{2}\right]_y^T \overline{u} \quad . \tag{2-4}$$

An inspection of Figure 6 shows that the (X_e, Y_e, Z_e) triad can be aligned with the (U_e, V_e, W_e) triad by these same two rotations. This means that

$$\overline{u}_e = \begin{bmatrix} u_e \\ v_e \\ w_e \end{bmatrix} = \left[\varphi_o - \frac{\pi}{2}\right]_y \left[A_z\right]_x \begin{bmatrix} x_e \\ y_e \\ z_e \end{bmatrix} = \left[\varphi_o - \frac{\pi}{2}\right]_y \left[A_z\right]_x \overline{x}_e \tag{2-5}$$

and

$$\overline{x}_e = \left[A_z\right]_x^T \left[\varphi_o - \frac{\pi}{2}\right]_y^T \overline{u}_e \quad . \tag{2-6}$$

Only one rotation is required to align the (U, V, W) triad with the (U_e, V_e, W_e) triad (Figure 8). Thus,

$$\overline{u}_e = \begin{bmatrix} u_e \\ v_e \\ w_e \end{bmatrix} = \left[\omega_e t\right]_x \begin{bmatrix} u \\ v \\ w \end{bmatrix} = \left[\omega_e t\right]_x \overline{u} \tag{2-7}$$

and

$$\overline{u} = \left[\omega_e t\right]_x^T \overline{u}_e \quad . \tag{2-8}$$

The necessary transformations are now available to develop a transformation from the surface triad to the launch-point triad. From equations (2-1), (2-6), and (2-7),

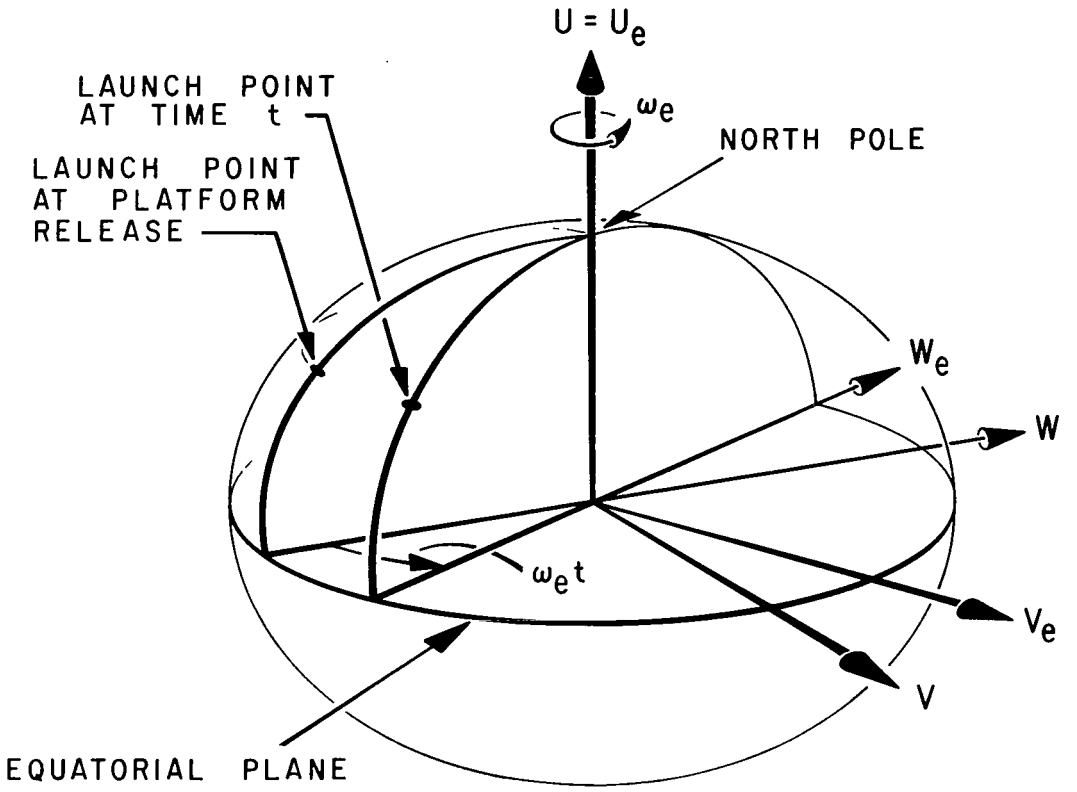

ω_e MAGNITUDE OF EARTH'S ROTATIONAL VELOCITY

t TIME FROM VEHICLE PLATFORM RELEASE

FIG. 8. ROTATION OF THE EARTH

$$\bar{x}_e = \left[A_z\right]_x^T \left[\varphi_o - \frac{\pi}{2}\right]_y^T \left[\omega_e t\right]_x \left[\varphi_o - \frac{\pi}{2}\right]_y \left[A_z\right]_x \bar{x}_s$$

or

$$\bar{x}_e = [TSE]\,\bar{x}_s \quad , \tag{2-9}$$

where

$$[TSE] = \left[A_z\right]_x^T \left[\varphi_o - \frac{\pi}{2}\right]_y^T \left[\omega_e t\right]_x \left[\varphi_o - \frac{\pi}{2}\right]_y \left[A_z\right]_x \quad .$$

The symbol TSE was chosen as an abbreviation for transformation from the space-fixed surface triad to the earth-fixed launch-point triad. Since [TSE] is a product of orthogonal matrices, [TSE] is orthogonal. Therefore,

$$\bar{x}_s = [TSE]^T \bar{x}_e \quad . \tag{2-10}$$

Selection of the surface triad to simulate the inertial platform system requires that a transformation be established from this triad to the vehicle system. In addition, this transformation must be a function of the simulated platform gimbal readings. The three right-hand rotations required to revolve the inertial platform triad to the same orientation as the vehicle triad were given in the discussion of Eulerian angles in Chapter I. Hence, the transformation in question is a product of the transformations of those three right-hand rotations. That is,

$$x_m = \begin{bmatrix} x_m \\ y_m \\ z_m \end{bmatrix} = \left[\varphi_r\right]_x \left[\varphi_y\right]_z \left[\varphi_p\right]_y \begin{bmatrix} x \\ y \\ z \end{bmatrix} = [TSM]\,\bar{x} \quad ,$$

where

$$[TSM] = \left[\varphi_r\right]_x \left[\varphi_y\right]_z \left[\varphi_p\right]_y \quad .$$

Since the (X_s, Y_s, Z_s) triad has the same orientation as the (X, Y, Z) triad,

$$\overline{x}_m = [TSM]\,\overline{x}_s \tag{2-11}$$

and

$$\overline{x}_s = [TSM]^T\,\overline{x}_m \quad . \tag{2-12}$$

This is the last transformation required by the total model.

CHAPTER III

EQUATIONS OF MOTION

The purpose of the total mathematical model is to determine the relative motion of a Saturn vehicle during the first stage of powered flight. The model is required to predict the vehicle's translational motion with respect to the launch point, the space-fixed position and velocity which the launch vehicle digital computer would compute, and the three Eulerian angles which the vehicle's inertial platform would measure. To accomplish the first two objectives, all translational motion of the vehicle is first referred to the space-fixed surface triad. Next, translational motion of the earth-fixed launch point triad is determined with respect to the surface triad. Earth-fixed motion of the vehicle is then obtained by algebraically combining the space-fixed translational motion of the launch-point triad with the space-fixed translation motion of the vehicle. To predict the three Eulerian angles, the angular motion of the vehicle is first computed with respect to the vehicle-fixed triad. This motion is transformed to Eulerian angular motion and integrated to obtain Eulerian angles.

Since most of the equations of motion involve vectorial quantities such as position, velocity, and acceleration, vectorial notation is used extensively

in this chapter. A subscript is attached to each vector to indicate the triad to which the vector components refer. The subscripts s, c, u, ue, e, and m are used to refer to the surface, earth-centered, equatorial, earth-equatorial, launch-point and vehicle triads, respectively. Since the surface triad and the earth-centered triad have the same orientation, a vector referred to either triad has the same components.

The equations that describe the translational motion of the launch-point triad with respect to the surface triad will be derived first. Figure 9 shows the relative position of the two triads for arbitrary t (the time from inertial platform release). Notice that

$$|\overline{R}(t)| = |\overline{R}(t=0)| = R(\psi_o) \quad ,$$

since the launch point remains on the Fischer Ellipsoid at a fixed geocentric latitude ψ_o. The following three equations are obtained from an inspection of Figure 9:

$$R(\psi_o) = \left[\frac{a^2}{\cos^2 \psi_o + \left(\frac{a}{b} \sin \psi_o \right)^2} \right]^{\frac{1}{2}} \tag{3-1}$$

$$\overline{RP}_s = \overline{R}(t)_s - \overline{R}(t=0)_s \tag{3-2}$$

$$\overline{R}(t)_{ue} = \begin{bmatrix} R(\psi_o) \sin \psi_o \\ 0 \\ -R(\psi_o) \cos \psi_o \end{bmatrix}_{ue} \tag{3-3}$$

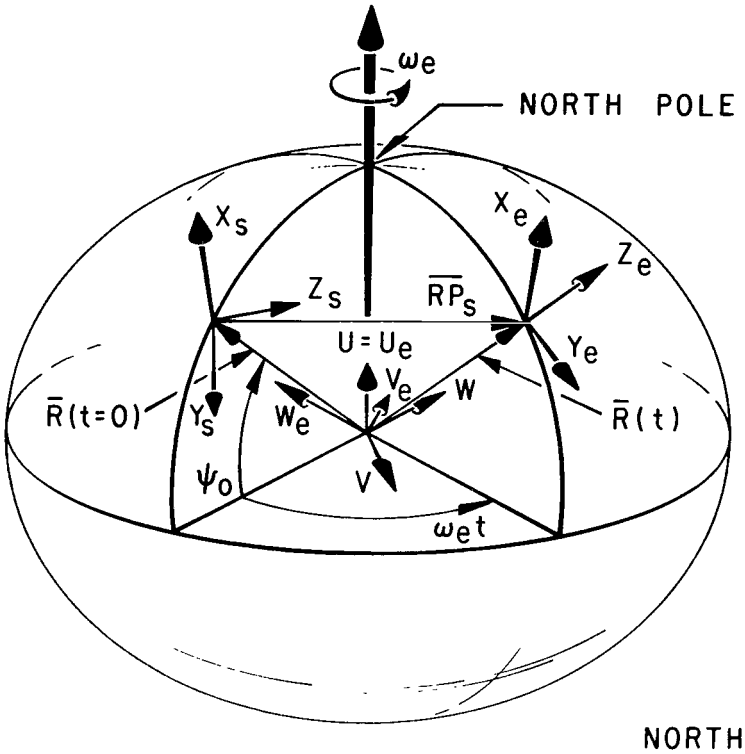

INTERSECTION OF FISHER ELLIPSOID AND PLANE CONTAINING THE LAUNCH POINT MERIDIAN AT INERTIAL PLATFORM RELEASE

$$\frac{\tilde{x}^2}{a^2} + \frac{\tilde{y}^2}{b^2} = 1$$

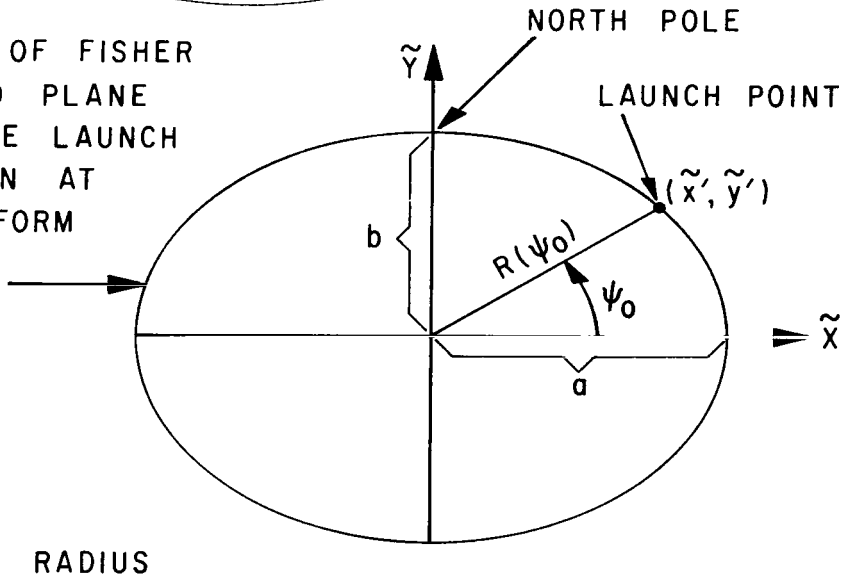

a - EQUATORIAL RADIUS OF EARTH

b - POLAR RADIUS OF EARTH

$$\tilde{x}' = R(\psi_0) \cos \psi_0$$

$$\tilde{y}' = R(\psi_0) \sin \psi_0$$

FIG. 9. RELATIVE POSITION OF SURFACE TRIAD AND LAUNCH POINT TRIAD

By equations (2-2), (2-8), and (3-3)

$$\overline{R}(t)_s = \left[A_z\right]_x^T \left[\varphi_o - \frac{\pi}{2}\right]_y^T \left[\omega_e t\right]_x^T \begin{bmatrix} R(\psi_o)\sin\psi_o \\ 0 \\ -R(\psi_o)\cos\psi_o \end{bmatrix}_{ue}$$

$$= \left[A_z\right]_x^T \left[\varphi_o - \frac{\pi}{2}\right]_y^T \begin{bmatrix} R(\psi_o)\sin\psi_o \\ R(\psi_o)\cos\psi_o \sin(\omega_e t) \\ -R(\psi_o)\cos\psi_o \cos(\omega_e t) \end{bmatrix}_{ue} . \qquad (3\text{-}4)$$

Then, substituting equation (3-4) into equation (3-2) yields

$$\overline{RP}_s = \left[A_z\right]_x^T \left[\varphi_o - \frac{\pi}{2}\right]_y^T \left\{ R(\psi_o) \begin{bmatrix} \sin\psi_o \\ \cos\psi_o \sin(\omega_e t) \\ -\cos\psi_o \cos(\omega_e t) \end{bmatrix}_{ue} - R(\psi_o) \begin{bmatrix} \sin\psi_o \\ 0 \\ -\cos\psi_o \end{bmatrix}_{ue} \right\}$$

$$= \left[A_z\right]_x^T \left[\varphi_o - \frac{\pi}{2}\right]_y^T \begin{bmatrix} 0 \\ R(\psi_o)\cos\psi_o \sin(\omega_e t) \\ R(\psi_o)\cos\psi_o (1 - \cos\omega_e t) \end{bmatrix}_{ue} . \qquad (3\text{-}5)$$

Since the product $\left[A_z\right]_x^T \left[\varphi_o - \frac{\pi}{2}\right]_y^T$ is constant with respect to time,

$$\dot{\overline{RP}}_s = \frac{d}{dt}(\overline{RP}_s) = \left[A_z\right]_x^T \left[\varphi_o - \frac{\pi}{2}\right]_y^T \begin{bmatrix} 0 \\ \omega_e R(\psi_o) \cos\psi_o \cos(\omega_e t) \\ \omega_e R(\psi_o) \cos\psi_o \sin(\omega_e t) \end{bmatrix}_{ue} . \quad (3\text{-}6)$$

Equations (3-5) and (3-6) above describe the translational motion of the launch-point triad with respect to the surface triad, as required.

The first law of motion of Newtonian mechanics is used to describe the translational motion of the vehicle center of gravity. This law states that a particle of mass m, subject to a force $\overline{F}$, moves relative to a basic frame of reference in accordance with the equation

$$\overline{F} = km\overline{A} \quad , \quad (3\text{-}7)$$

where $\overline{A}$ is the acceleration of the particle and k is the universal positive constant that depends on the choice of units of force, mass, length, and time. In the model being described, it is assumed that a system of units is used for which $k = 1$. The frame of reference to which motion of the vehicle CG is referred is the space-fixed surface triad.

Notice that neither m nor $\overline{F}$ is constant in the model. Mass is a function of the rate at which the vehicle's engines consume the stored propellant. $\overline{F}$ depends on the magnitude and direction of the engines' thrust, local atmospheric conditions, velocity of the vehicle with respect to the air, and

attitude of the vehicle. The forces that act upon the vehicle are described in Chapter IV.

Equation (3-7) gives, on resolution into components along the surface triad axes,

$$m\frac{d^2X_s}{dt^2} = F_{xs} \quad , \quad m\frac{d^2Y_s}{dt^2} = F_{ys} \quad , \quad m\frac{d^2Z_s}{dt^2} = F_{zs} \quad ,$$

where F_{xs} , F_{ys} , and F_{zs} are the components of force along the axes. These three equations are each solved for acceleration and integrated to obtain velocity. That is, for arbitrary t ,

$$\frac{dX_s}{dt} = \left(\frac{dX_s}{dt}\right)_{t=0} + \int_0^t \frac{F_{xs}}{m}\, dt \quad , \tag{3-8}$$

$$\frac{dY_s}{dt} = \left(\frac{dY_s}{dt}\right)_{t=0} + \int_0^t \frac{F_{ys}}{m}\, dt \quad , \tag{3-9}$$

and

$$\frac{dZ_s}{dt} = \left(\frac{dZ_s}{dt}\right)_{t=0} + \int_0^t \frac{F_{zs}}{m}\, dt \quad . \tag{3-10}$$

Position of the vehicle at arbitrary t is determined by integrating equations (3-8), (3-9), and (3-10).

$$XS_p = \left(XS_p\right)_{t=0} + \int_0^t \left(\frac{dX_s}{dt}\right) dt \tag{3-11}$$

$$YS_p = \left(YS_p\right)_{t=0} + \int_0^t \left(\frac{dY_s}{dt}\right) dt \tag{3-12}$$

$$ZS_p = \left(ZS_p\right)_{t=0} + \int_0^t \left(\frac{dZ_s}{dt}\right) dt \tag{3-13}$$

The symbol used for this position vector is

$$\overline{RS}_s = \begin{bmatrix} XS_p \\ YS_p \\ ZS_p \end{bmatrix}_s .$$

For a length of time Δ after the inertial platform is released, a Saturn vehicle does not move from its launch pad. For this reason, a second time reference, $\tau = t - \Delta$, is defined. If $\tau \leq 0$, the vehicle CG has a constant velocity because of the earth's rotation. Figure 10 shows the relative position of the vehicle for $0 \leq t \leq \Delta$. During this time,

$$\overline{RS}_s = \overline{RP}_s + \left[TSE\right]^T \overline{REO}_e \tag{3-14}$$

and

$$\dot{\overline{RS}}_s = \frac{d}{dt}\left(\overline{RS}_s\right) = \left(\overline{\omega}_e\right)_s \times \overline{RC}_s \tag{3-15}$$

where

$$\left(\overline{\omega}_e\right)_s = \left[A_z\right]_x^T \left[\varphi_o - \frac{\pi}{2}\right]_y^T \begin{bmatrix} \omega_e \\ 0 \\ 0 \end{bmatrix}_u \tag{3-16}$$

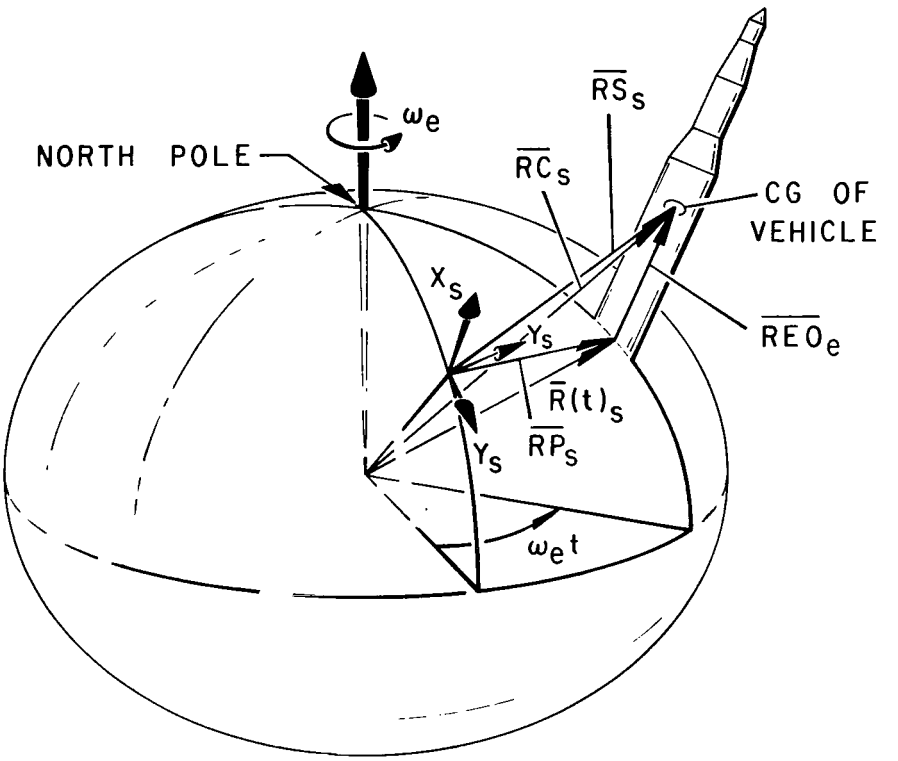

FIG. 10. RELATIVE POSITION OF A VEHICLE BEFORE LAUNCH

and

$$\overline{RC}_s = \overline{R}(t)_s + [TSE]^T \overline{REO}_e \quad . \tag{3-17}$$

Equations (3-14) and (3-15) are not valid for $\tau > 0$. Figure 11 shows the relative position of the CG after first motion. At this time,

$$\overline{RE}_e = [TSE](\overline{RS}_s - \overline{RP}_s) \tag{3-18}$$

and

$$\overline{RS}_s = \overline{RP}_s + [TSE]^T \overline{RE}_e \quad . \tag{3-19}$$

By differentiating equation (3-19), an expression is obtained that contains the velocity of the CG with respect to the launch point triad.

$$\frac{d}{dt}(\overline{RS}_s) = \frac{d}{dt}(\overline{RP}_s) + \left(\frac{d}{dt}[TSE]^T\right)\overline{RE}_e + [TSE]^T\left(\frac{d}{dt}\overline{RE}_e\right)$$

This equation can be solved for $\frac{d}{dt}(\overline{RE}_e)$ by transposing terms and multiplying each one by $[TSE]$.

$$\begin{aligned}\frac{d}{dt}\overline{RE}_e &= [TSE]\frac{d}{dt}(\overline{RS}_s - \overline{RP}_s) - [TSE]\left(\frac{d}{dt}[TSE]^T\right)\overline{RE}_e \\ &= [TSE](\dot{\overline{RS}}_s - \dot{\overline{RP}}_s) - [TSE]\left(\frac{d}{dt}[TSE]^T\right)\overline{RE}_e\end{aligned} \tag{3-20}$$

All the terms in equation (3-20) have been previously defined except $\frac{d}{dt}[TSE]^T$. An expression for this term will now be derived.

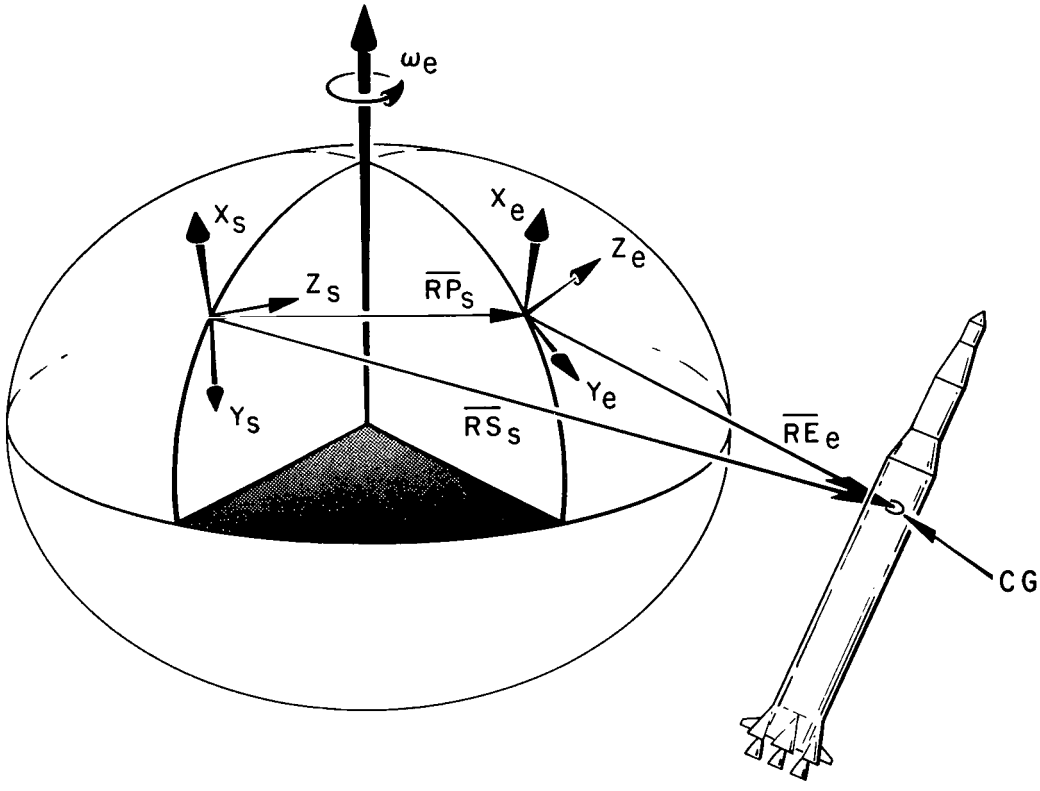

FIG. 11. RELATIVE POSITION OF A VEHICLE AFTER LAUNCH

Define I_s, J_s, K_s to be unit vectors along the X_s, Y_s, Z_s axes and I_e, J_e, K_e to be unit vectors along the X_e, Y_e, Z_e axes. By equation (2-10), these two unit triads are related by the equation

$$\begin{bmatrix} I_s \\ J_s \\ K_s \end{bmatrix} = [TSE]^T \begin{bmatrix} I_e \\ J_e \\ K_e \end{bmatrix} . \tag{3-21}$$

Notice that the derivatives of the unit vectors I_e, J_e, K_e are nonzero since their directions continuously change because of the earth's rotational velocity. Hence,

$$\frac{d\bar{\eta}}{dt} = \left(\bar{\omega}_e\right)_e \times \bar{\eta} \tag{3-22}$$

for $\bar{\eta} = I_e, J_e, K_e$ where

$$\left(\bar{\omega}_e\right)_e = \left[A_z\right]_X^T \left[\varphi_o - \frac{\pi}{2}\right]_y^T \begin{bmatrix} \omega_e \\ 0 \\ 0 \end{bmatrix}_{ue} = \begin{bmatrix} \omega_{e1} \\ \omega_{e2} \\ \omega_{e3} \end{bmatrix}_e . \tag{3-23}$$

By defining $[TSE] = [A_{ij}]$ where $i, j = 1, 2, 3$, equation (3-21) can be rewritten in component form as

$$I_s = A_{11} I_e + A_{21} J_e + A_{31} K_e$$

$$J_s = A_{12} I_e + A_{22} J_e + A_{32} K_e$$

$$K_s = A_{13} I_e + A_{23} J_e + A_{33} K_e$$

An application of equation (3-22) and the fact that the unit vectors I_s, J_s, and K_s do not vary with time yield expressions that contain the derivatives of all the elements of [TSE] .

$$\frac{dI_s}{dt} = \bar{0} = \dot{A}_{11} I_e + \dot{A}_{21} J_e + \dot{A}_{31} K_e + \left(\bar{\omega}_e\right)_e \times (A_{11} I_e + A_{21} J_e + A_{31} K_e) \quad , \tag{3-24}$$

$$\frac{dJ_s}{dt} = \bar{0} = \dot{A}_{12} I_e + \dot{A}_{22} J_e + \dot{A}_{32} K_e + \left(\bar{\omega}_e\right)_e \times (A_{12} I_e + A_{22} J_e + A_{32} K_e) \quad , \tag{3-25}$$

and

$$\frac{dK_s}{dt} = \bar{0} = \dot{A}_{13} I_e + \dot{A}_{23} J_e + \dot{A}_{33} K_e + \left(\bar{\omega}_e\right)_e \times (A_{13} I_e + A_{23} J_e + A_{33} K_e) \quad , \tag{3-26}$$

where

$$\dot{A}_{ij} = \frac{d}{dt} A_{ij} \quad .$$

By carrying out the indicated cross product and collecting terms, equation (3-24) becomes

$$\bar{0} = (\dot{A}_{11} + \omega_{e2} A_{31} - \omega_{e3} A_{21}) I_e + (\dot{A}_{21} + \omega_{e3} A_{11} - \omega_{e1} A_{31}) J_e + (\dot{A}_{31} + \omega_{e1} A_{21} - \omega_{e2} A_{11}) K_e \quad . \tag{3-27}$$

The vectors I_e, J_e, and K_e are linearly independent since they are mutually orthogonal. Hence,

$$\dot{A}_{11} = \omega_{e3} A_{21} - \omega_{e2} A_{31} \quad ,$$

$$\dot{A}_{21} = \omega_{e1} A_{31} - \omega_{e3} A_{11} \quad ,$$

and

$$\dot{A}_{31} = \omega_{e2} A_{11} - \omega_{e1} A_{21} \quad .$$

An application of the above procedure to equations (3-25) and (3-26) yields expressions for $\dot{A}_{ij}$ where $i = 1, 2, 3$ and $j = 2, 3$. These expressions are:

$$\dot{A}_{12} = \omega_{e3} A_{22} - \omega_{e2} A_{32}$$

$$\dot{A}_{22} = \omega_{e1} A_{32} - \omega_{e3} A_{12}$$

$$\dot{A}_{32} = \omega_{e2} A_{12} - \omega_{e1} A_{22}$$

$$\dot{A}_{13} = \omega_{e3} A_{23} - \omega_{e2} A_{33}$$

$$\dot{A}_{23} = \omega_{e1} A_{33} - \omega_{e3} A_{13}$$

$$\dot{A}_{33} = \omega_{e2} A_{13} - \omega_{e1} A_{23} \quad .$$

Using the above equations, we can now express the time derivative of [TSE] as

$$\frac{d}{dt}[\mathrm{TSE}] = \begin{bmatrix} \dot{A}_{11} & \dot{A}_{12} & \dot{A}_{13} \\ \dot{A}_{21} & \dot{A}_{22} & \dot{A}_{23} \\ \dot{A}_{31} & \dot{A}_{32} & \dot{A}_{33} \end{bmatrix}$$

$$= \begin{bmatrix} \omega_{e3}A_{21} - \omega_{e2}A_{31} & \omega_{e3}A_{22} - \omega_{e2}A_{32} & \omega_{e3}A_{23} - \omega_{e2}A_{33} \\ \omega_{e1}A_{31} - \omega_{e3}A_{11} & \omega_{e1}A_{32} - \omega_{e3}A_{12} & \omega_{e1}A_{33} - \omega_{e3}A_{13} \\ \omega_{e2}A_{11} - \omega_{e1}A_{21} & \omega_{e2}A_{12} - \omega_{e1}A_{22} & \omega_{e2}A_{13} - \omega_{e1}A_{23} \end{bmatrix}$$

$$= \begin{bmatrix} 0 & \omega_{e3} & -\omega_{e2} \\ -\omega_{e3} & 0 & \omega_{e1} \\ \omega_{e2} & -\omega_{e1} & 0 \end{bmatrix} \begin{bmatrix} A_{11} & A_{12} & A_{13} \\ A_{21} & A_{22} & A_{23} \\ A_{31} & A_{32} & A_{33} \end{bmatrix}$$

$$= [\Phi][TSE] \quad , \tag{3-28}$$

where

$$[\Phi] = \begin{bmatrix} 0 & \omega_{e3} & -\omega_{e2} \\ -\omega_{e3} & 0 & \omega_{e1} \\ \omega_{e2} & -\omega_{e1} & 0 \end{bmatrix} \quad .$$

Therefore,

$$\frac{d}{dt}[TSE]^T = \left(\frac{d}{dt}[TSE]\right)^T = \left([\Phi][TSE]\right)^T = [TSE]^T[\Phi]^T \quad . \tag{3-29}$$

By substituting equation (3-29) into equation (3-20), $\frac{d}{dt}(RE_e) = \dot{\overline{RE}}_e$ can be be expressed as

$$\dot{\overline{RE}}_e = [TSE](\dot{\overline{RS}}_s - \dot{\overline{RP}}_s) - [\Phi]^T\overline{RE}_e$$

$$= [TSE](\dot{\overline{RS}}_s - \dot{\overline{RP}}_s) - \left(\overline{\omega}_e\right)_e \times \overline{RE}_e \quad . \tag{3-30}$$

Equations (3-18) and (3-30) describe the relative translational motion of the vehicle CG with respect to the launch-point triad as required.

Total motion of a vehicle is described by the model in terms of the translational motion of its CG and rotational motion of the vehicle about its CG. The equations that describe the second type of motion are all that remain to be derived.

The model assumes a vehicle to be a rigid body constrained to rotate about its CG. Thus, the angular momentum about the CG is

$$\overline{L} = I_x \omega_x i + I_y \omega_y j + I_z \omega_z k \quad , \tag{3-31}$$

where i, j, k are unit vectors along the X_m, Y_m, Z_m axes, respectively; I_x, I_y, I_z are the principal moments of inertia about these axes; and ω_x, ω_y, ω_z are the components of angular velocity $\overline{\omega}$ of the vehicle about these axes. Here, $\overline{\omega}$ is the angular velocity of the vehicle triad with respect to the surface triad. Equation (3-31) is classical and can be found in most books on Newtonian mechanics.

The total moment of the external forces about the CG is

$$\begin{aligned}\overline{M} = \frac{d\overline{L}}{dt} = {} & (\dot{I}_x \omega_x + I_x \dot{\omega}_x) i + (\dot{I}_y \omega_y + I_y \dot{\omega}_y) j \\ & + (\dot{I}_z \omega_z + I_z \dot{\omega}_z) k + I_x \omega_x \frac{di}{dt} \\ & + I_y \omega_y \frac{dj}{dt} + I_z \omega_z \frac{dk}{dt}\end{aligned} \tag{3-32}$$

where

$$\dot{I}_\eta = \frac{dI_\eta}{dt} ,$$

$$\dot{\omega}_\eta = \frac{d\omega_\eta}{dt}$$

for $\eta = x, y, z$.

Since the time rate of change of the principal moments of inertia is very small, it is assumed that $\dot{I}_\eta = 0$ for $\eta = x,y,z$. Each of the unit vectors i, j, k changes only in direction so that

$$\frac{d\bar{\eta}}{dt} = \overline{\omega}_m \times \bar{\eta} \qquad \text{for} \quad \bar{\eta} = i, j, k \quad .$$

Thus, equation (3-32) can now be simplified to

$$\overline{M} = I_x \dot{\omega}_x i + I_y \dot{\omega}_y j + I_z \dot{\omega}_z k + \overline{\omega}_e \times (I_x \omega_x i + I_y \omega_y j + I_z \omega_z k)$$

$$= \left[I_x \dot{\omega}_x - \omega_y \omega_z (I_y - I_z)\right] i + \left[I_y \dot{\omega}_y - \omega_x \omega_z (I_z - I_x)\right] j$$

$$+ \left[I_z \dot{\omega}_z - \omega_x \omega_y (I_x - I_y)\right] k \quad .$$

This equation can be rewritten in component form as

$$M_1 = I_x \dot{\omega}_x - \omega_y \omega_z (I_y - I_z)$$

$$M_2 = I_y \dot{\omega}_y - \omega_x \omega_z (I_z - I_y)$$

$$M_3 = I_z \dot{\omega}_z - \omega_x \omega_y (I_x - I_y)$$

where M_1, M_2, M_3 are the components of $\overline{M}$ along i, j, k . Therefore,

$$\dot{\overline{\omega}}_m = \begin{bmatrix} \dot{\omega}_x \\ \dot{\omega}_y \\ \dot{\omega}_z \end{bmatrix} = \begin{bmatrix} M_1/I_x + \omega_y\omega_z(I_y - I_z)/I_x \\ M_2/I_y + \omega_x\omega_z(I_z - I_y)/I_y \\ M_3/I_z + \omega_x\omega_y(I_x - I_y)/I_z \end{bmatrix}_m \quad . \tag{3-33}$$

An expression for the total moment vector, $\overline{M}$, about the vehicle CG is given in Chapter IV. Angular velocity of a vehicle about its CG is determined at arbitrary t by integrating equation (3-33) to obtain

$$\overline{\omega}_m = \left(\overline{\omega}_m\right)_{t=0} + \int_0^t \dot{\overline{\omega}}_m \, dt \tag{3-34}$$

where

$$\left(\overline{\omega}_m\right)_{t=0} = [\text{TSM}] \left(\overline{\omega}_e\right)_s$$

Equations (3-33) and (3-34) describe the rotational motion of a vehicle about its CG as required.

Since the orientation of a Saturn vehicle is defined by three Eulerian angles, some method of computing these angles must be established. One of the simplest methods is to transform the vehicle angular velocity to Eulerian angular velocity and integrate the Eulerian angular velocity to obtain Eulerian angles. To this end, a transformation from the vehicle angular velocity to Eulerian angular velocity will now be derived.

The required transformation will be derived from infinitesimal rotations of a vehicle about its CG. Suppose that a rigid vehicle has turned through

an infinitesimal angle about an axis through its CG. This infinitesimal rotation may be represented by an infinitesimal vector $\delta\bar{\eta}$ (Figure 12). $\delta\bar{\eta}$ determines the displacements of all points of the vehicle.

Let $\bar{r}$ be the position vector relative to the CG of a point A before the displacement and $\bar{r} + \delta\bar{r}$ the position vector after displacement. In the rotation $\delta\bar{\eta}$ the point A moves perpendicular to the plane containing the vectors $\bar{r}$ and $\delta\bar{\eta}$, in the same direction as the vector product $\delta\bar{\eta} \times \bar{r}$. The magnitude of $\delta\bar{r}$ is $|\delta\bar{\eta}|\,AB = |\delta\bar{\eta}|\,|\bar{r}|\sin\theta$ (Figure 12). Hence,

$$\delta\bar{r} = \delta\bar{\eta} \times \bar{r} \quad . \tag{3-35}$$

Infinitesimal rotations about a point can be added vectorially. Let $\delta\bar{\eta}$ and $\delta\bar{m}$ be two infinitesimal rotations applied in succession about axes through the vehicle CG. Then the position vector of a point A in the vehicle is $\bar{r}$ before displacement, $\bar{r} + \delta\bar{\eta} \times \bar{r}$ after the $\delta\bar{\eta}$ rotation, and $\bar{r} + \delta\bar{\eta} \times \bar{r} + \delta\bar{m} \times (\bar{r} + \delta\bar{\eta} \times \bar{r})$ after the $\delta\bar{m}$ rotation. By neglecting infinitesimals of the second order, the resultant displacement of point A is

$$\delta\bar{\eta} \times \bar{r} + \delta\bar{m} \times \bar{r} = (\delta\bar{\eta} + \delta\bar{m}) \times \bar{r} \quad . \tag{3-36}$$

Thus, an infinitesimal rotation of a vehicle about its CG may be described either as an infinitesimal rotation $\delta\bar{\eta}$ or by means of infinitesimal increments in the Eulerian angles. The rotation of a vehicle from the orientation $(\varphi_p, \varphi_y, \varphi_r)$ to a second orientation $(\varphi_p + \Delta\varphi_p, \varphi_y + \Delta\varphi_y, \varphi_r + \Delta\varphi_r)$ may be accomplished by applying the following finite rotations in order:

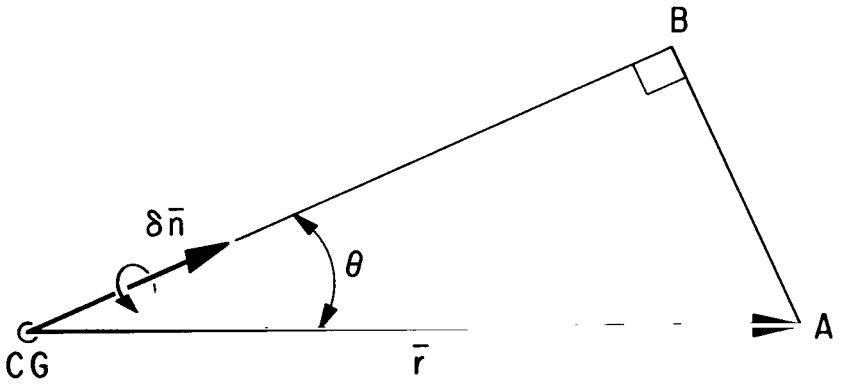

FIG. 12. INFINITESIMAL ROTATION

$\Delta\varphi_r i$, $\Delta\varphi_y K'$, $\Delta\varphi_p J$ where i, K', and J are unit vectors along the X_m, Z', and Y axes, respectively. (See Figure 3 of Chapter I.) If the increments in the Eulerian angles are infinitesimal, the order of these rotations is immaterial, so that

$$\delta\bar{\eta} = \Delta\varphi_r i + \Delta\varphi_p J + \Delta\varphi_y K' \quad . \tag{3-37}$$

The infinitesimal rotation of concern here is the rotation $|\bar{\omega}|\,dt$ in the direction of the unit vector $\bar{\omega}/|\bar{\omega}|$ where $\bar{\omega}$ is the angular velocity vector of the vehicle. Corresponding to this rotation, $(|\bar{\omega}|\,dt)\,(\bar{\omega}/|\bar{\omega}|) = \bar{\omega}\,dt$, are the three infinitesimal increments to the Eulerian angles, $d\varphi_r i$, $d\varphi_p J$, $d\varphi_y K'$. Thus, equation (3-37) becomes

$$\bar{\omega}\,dt = d\varphi_r i + d\varphi_p J + d\varphi_y K' \quad . \tag{3-38}$$

By dividing each term of equation (3-38) by dt, the expression

$$\bar{\omega} = \dot{\varphi}_r i + \dot{\varphi}_p J + \dot{\varphi}_y K' \tag{3-39}$$

is obtained where $\dot{\varphi}_m = \dfrac{d\varphi_m}{dt}$ for $m = r, p, y$. It is now convenient to convert equation (3-39) to an expression involving unit vectors along the X, Y, and Z axes of Figure 3. Define j, k, I', J', I, and K to be unit vectors along the Y_m, Z_m, X', Y', X, and Z axes, respectively. Then, by an inspection of Figure 3, we see

$$\begin{bmatrix} I' \\ J \\ K' \end{bmatrix} = \left[\varphi_p\right]_y \begin{bmatrix} I \\ J \\ K \end{bmatrix} , \tag{3-40}$$

and

$$\begin{bmatrix} i \\ J' \\ K' \end{bmatrix} = \left[\varphi_y\right]_z \begin{bmatrix} I' \\ J \\ K' \end{bmatrix} . \tag{3-41}$$

From these two equations, it is easy to show that

$$i = \cos\varphi_y \cos\varphi_p I + \sin\varphi_y J - \cos\varphi_y \sin\varphi_p K \tag{3-42}$$

and

$$K' = \sin\varphi_p I + \cos\varphi_p K . \tag{3-43}$$

Then, by substituting equations (3-42) and (3-43) into equation (3-39) and simplifying, we obtain

$$\overline{\omega}_s = (\dot{\varphi}_r \cos\varphi_y \cos\varphi_p + \dot{\varphi}_y \sin\varphi_p) I + (\dot{\varphi}_r \sin\varphi_y + \dot{\varphi}_p) J + (\dot{\varphi}_y \cos\varphi_p - \dot{\varphi}_r \cos\varphi_y \sin\varphi_p) K . \tag{3-44}$$

A resolution of $\overline{\omega}$ in the vehicle system can now be obtained by using equation (2-11):

$$\overline{\omega}_m = [TSM] \begin{bmatrix} \dot{\varphi}_r \cos \varphi_y \cos \varphi_p + \dot{\varphi}_y \sin \varphi_p \\ \dot{\varphi}_r \sin \varphi_y + \dot{\varphi}_p \\ \dot{\varphi}_y \cos \varphi_p - \dot{\varphi}_r \cos \varphi_y \sin \varphi_p \end{bmatrix}$$

$$= \begin{bmatrix} \dot{\varphi}_p \sin \varphi_y + \dot{\varphi}_r \\ \dot{\varphi}_y \sin \varphi_r + \dot{\varphi}_p \cos \varphi_r \cos \varphi_y \\ \dot{\varphi}_y \cos \varphi_r - \dot{\varphi}_p \sin \varphi_r \cos \varphi_y \end{bmatrix}$$

$$= \begin{bmatrix} \sin \varphi_p & 0 & 1 \\ \cos \varphi_r \cos \varphi_y & \sin \varphi_r & 0 \\ -\sin \varphi_r \cos \varphi_y & \cos \varphi_r & 0 \end{bmatrix} \begin{bmatrix} \dot{\varphi}_p \\ \dot{\varphi}_y \\ \dot{\varphi}_r \end{bmatrix}$$

$$= [TEM] \begin{bmatrix} \dot{\varphi}_p \\ \dot{\varphi}_y \\ \dot{\varphi}_r \end{bmatrix} \qquad (3\text{-}45)$$

where

$$[TEM] = \begin{bmatrix} \sin \varphi_p & 0 & 1 \\ \cos \varphi_r \cos \varphi_y & \sin \varphi_r & 0 \\ -\sin \varphi_r \cos \varphi_y & \cos \varphi_r & 0 \end{bmatrix} .$$

Here, the symbol TEM was chosen to stand for the transformation from Eulerian angular rates to vehicle angular rates. The inverse of [TEM] can be computed by multiplying the transpose of the matrix of cofactors of [TEM]

by the scalar $1/|[TEM]|$, where $|[TEM]|$ is the value of the determinant of [TEM] . Thus,

$$[TEM]^{-1} = \frac{1}{\cos \varphi_y} \begin{bmatrix} 0 & 0 & \cos \varphi_y \\ \cos \varphi_r & \sin \varphi_r \cos \varphi_y & -\sin \varphi_y \cos \varphi_r \\ -\sin \varphi_r & \cos \varphi_r \cos \varphi_y & \sin \varphi_y \sin \varphi_r \end{bmatrix}^T$$

$$= \begin{bmatrix} 0 & \cos \varphi_r \sec \varphi_y & -\sin \varphi_r \sec \varphi_y \\ 0 & \sin \varphi_r & \cos \varphi_r \\ 1 & -\tan \varphi_y \cos \varphi_r & \tan \varphi_y \sin \varphi_r \end{bmatrix} . \qquad (3\text{-}46)$$

Therefore, $[TEM]^{-1}$ exists when $\varphi_y \neq \pm 90$ degrees, so that

$$\begin{bmatrix} \dot{\varphi}_p \\ \dot{\varphi}_y \\ \dot{\varphi}_r \end{bmatrix} = [TEM]^{-1} \begin{bmatrix} \omega_x \\ \omega_y \\ \omega_z \end{bmatrix} = [TEM]^{-1} \overline{\omega}_m . \qquad (3\text{-}47)$$

Since the yaw gimbal of a Saturn inertial platform is physically restricted to rotations of ± 45 degrees from its initial position, the above restrictions on φ_y create no problem.

Equation (3-47) is the required transformation for converting the vehicle angular velocity to Eulerian angular velocity. The Eulerian angles φ_p, φ_y and φ_r are computed at arbitrary t as follows:

$$\varphi_\eta = \left(\varphi_\eta\right)_{t=0} + \int_0^t \dot{\varphi}_\eta \, dt \qquad (3\text{-}48)$$

for $\eta = p, y, r$. This is the last equation required to describe the rotational motion of a rigid vehicle about its CG.

CHAPTER IV

FORCE AND MOMENT EQUATIONS

A Saturn vehicle experiences forces from three basic sources during its first stage of powered flight. These sources are the vehicle's first-stage engines and the earth's gravitational potential and atmosphere. This chapter provides the equations required to compute the total force and moment vectors that result from these forces.

The S-IC stage of a Saturn V vehicle has five engines (Figure 1) that propel the vehicle through the earth's atmosphere. The four outboard engines are attached to the base of the stage by mechanical joints that permit the engines to gimbal or rotate through a limited angle from their null position. Gimbaling of these four engines according to commands from the flight control computer forces the vehicle to follow the desired attitude commands. Each outboard engine has two hydraulic actuators, attached 90 degrees apart, that execute the flight control computer commands. One actuator provides attitude control in the pitch plane, and the other actuator provides attitude control in the yaw plane. Attitude control is achieved in the roll plane by moving both the pitch and yaw actuators in the proper directions.

In Chapter I, the word "control" was defined, and the control system was briefly described. A more detailed description of this system will accrue as the model for it is presented.

A block diagram of the control system for a Saturn vehicle is shown in Figure 13. Attitude error signals are computed in the LVDC from the platform gimbal angles and the commanded attitude angles. The vehicle angular velocities about the X_m, Y_m, and Z_m axes are measured by three rate gyroscopes. In the flight control computer, signals from the rate gyroscopes and the attitude error signals are electrically filtered, multiplied by a gain factor, and then combined to generate the commands to the four outboard engine actuators.

The commanded attitude angles χ_p, χ_y, and χ_r are defined to be the three Eulerian angles through which the inertial platform triad must be rotated to align it with the desired orientation of the vehicle. If i_c, j_c, and k_c are unit vectors along the vehicle X_m, Y_m, and Z_m axes, respectively, when the vehicle has the orientation (χ_p, χ_y, χ_r), then

$$\begin{bmatrix} i_c \\ j_c \\ k_c \end{bmatrix} = \left[\chi_r\right]_x \left[\chi_y\right]_z \left[\chi_p\right]_y \begin{bmatrix} I_s \\ J_s \\ K_s \end{bmatrix} = [TSC] \begin{bmatrix} I_s \\ J_s \\ K_s \end{bmatrix} \qquad (4\text{-}1)$$

where $[TSC] = \left[\chi_r\right]_x \left[\chi_y\right]_z \left[\chi_p\right]_y$ and I_s, J_s, and K_s are unit vectors along the surface triad X_s, Y_s, and Z_s axes respectively.

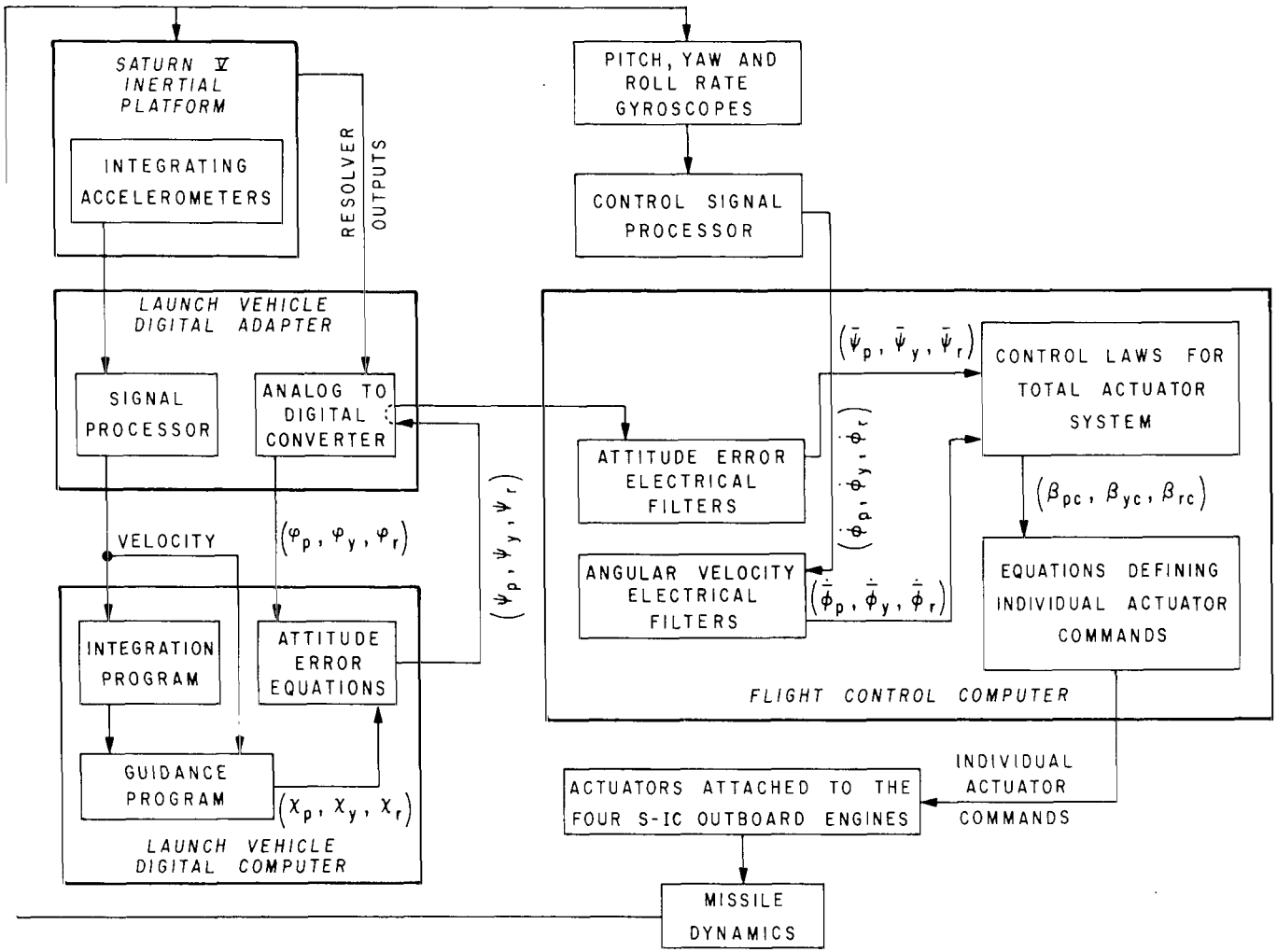

FIG. 13. SATURN CONTROL SYSTEM BLOCK DIAGRAM

Similarly, the attitude error signals ψ_p, ψ_y, and ψ_r are defined to be the three Eulerian angles through which the vehicle triad (X_m, Y_m, Z_m) must be rotated to align it with the (i_c, j_c, k_c) triad. Therefore,

$$\begin{bmatrix} i_c \\ j_c \\ k_c \end{bmatrix} = \left[\psi_r\right]_x \left[\psi_y\right]_z \left[\psi_p\right]_y \begin{bmatrix} i \\ j \\ k \end{bmatrix} \tag{4-2}$$

where i, j, and k are unit vectors along the vehicle X_m, Y_m, and Z_m axes respectively. By equations (2-12) and (4-1), a second expression for the transformation from the (X_m, Y_m, Z_m) triad to the (i_c, j_c, k_c) triad is obtained.

$$\begin{bmatrix} i_c \\ j_c \\ k_c \end{bmatrix} = [TSC][TSM]^T \begin{bmatrix} i \\ j \\ k \end{bmatrix} . \tag{4-3}$$

Hence, by equations (4-2) and (4-3),

$$\left[\psi_r\right]_x \left[\psi_y\right]_z \left[\psi_p\right]_y = [TSC][TSM]^T . \tag{4-4}$$

The following expressions for ψ_p, ψ_y, and ψ_r can be obtained from equation (4-4) by performing the indicated product and equating corresponding elements of the two matrices.

$$\psi_p = (\varphi_p - \chi_p) \cos\left(\frac{\varphi_y + \chi_y}{2}\right) \cos\left(\frac{\varphi_r + \chi_r}{2}\right) + (\varphi_y - \chi_y) \sin\left(\frac{\varphi_r + \chi_r}{2}\right) \tag{4-5}$$

$$\psi_y = (\varphi_y - \chi_y) \cos\left(\frac{\varphi_r + \chi_r}{2}\right)$$

$$- (\varphi_p - \chi_p) \cos\left(\frac{\varphi_y + \chi_y}{2}\right) \sin\left(\frac{\varphi_r + \chi_r}{2}\right) \qquad (4\text{-}6)$$

$$\psi_r = (\varphi_r - \chi_r) + (\varphi_p - \chi_p) \sin\left(\frac{\varphi_y + \chi_y}{2}\right) \qquad (4\text{-}7)$$

The details involved in deriving the above expressions and the approximations on which they are based are given in Reference 3. These are the expressions used by the LVDC for computing the attitude errors.

The attitude errors are converted to analogue signals by the LVDA before they reach the flight control computer. Here, both the attitude error signals and the angular velocity signals from the rate gyroscopes are passed through electrical networks called filters. These networks are designed to remove the effects of flexible body motion from the input signals and to maintain proper control system stability. In this paper the symbols $\overline{\psi}_p$, $\overline{\psi}_y$, $\overline{\psi}_r$ and $\dot{\overline{\phi}}_p$, $\dot{\overline{\phi}}_y$, $\dot{\overline{\phi}}_r$ are used to denote the filtered attitude error and angular velocity signals, respectively.

A special digital filtering technique (Reference 4) has been developed to simulate the electrical control filters. This technique will not be discussed in this paper since it is widely used and a discussion of it is lengthy.

The filtered attitude error and angular velocity signals are combined in the flight control computer by the following control laws to give the commanded thrust deflections in the pitch, yaw, and roll planes.

Pitch: $\beta_{pc} = A_{0p}\,\overline{\psi}_p + A_{1p}\,\dot{\overline{\phi}}_p$ (4-8)

Yaw: $\beta_{yc} = A_{0y}\,\overline{\psi}_y + A_{1y}\,\dot{\overline{\phi}}_y$ (4-9)

Roll: $\beta_{rc} = A_{0r}\,\overline{\psi}_r + A_{1r}\,\dot{\overline{\phi}}_r$ (4-10)

Here, $A_{0\eta}$ and $A_{1\eta}$ for $\eta = p, y, r$ are gain factors that provide stability to the control system. The magnitudes of these factors are specified as step functions of flight time.

Individual commands to the actuators of the four control engines are defined by the following equations:

$$\beta_{p1} = \beta_{pc} - \beta_{rc}/\sqrt{2} \quad (4\text{-}11)$$

$$\beta_{p2} = \beta_{pc} - \beta_{rc}/\sqrt{2} \quad (4\text{-}12)$$

$$\beta_{p3} = \beta_{pc} + \beta_{rc}/\sqrt{2} \quad (4\text{-}13)$$

$$\beta_{p4} = \beta_{pc} + \beta_{rc}/\sqrt{2} \quad (4\text{-}14)$$

$$\beta_{y1} = \beta_{yc} + \beta_{rc}/\sqrt{2} \quad (4\text{-}15)$$

$$\beta_{y2} = \beta_{yc} - \beta_{rc}/\sqrt{2} \quad (4\text{-}16)$$

$$\beta_{y3} = \beta_{yc} - \beta_{rc}/\sqrt{2} \quad (4\text{-}17)$$

$$\beta_{y4} = \beta_{yc} + \beta_{rc}/\sqrt{2} \quad , \quad (4\text{-}18)$$

where β_{pi} and β_{yi} are the commands to the pitch and yaw actuators of the i^{th} outboard engine.

The positive signs for all the control parameters are shown by Figure 1. A positive attitude error about a vehicle axis requires a negative right-hand rotation about that axis to correct for it. A positive angular velocity about a vehicle axis has the same sense as a positive right-hand rotation about that axis. The bases of the four outboard engines are moved parallel to the $+Z_m$ axis by a $+\beta_p$ creating a negative moment about the pitch or Y_m axis. Similarly, a $+\beta_y$ moves the base of the engines parallel to the negative Y_m axis, creating a negative moment about the yaw or Z_m axis. Thus, positive actuator movements correct for positive attitude errors.

The thrust vector of each of the five S-IC stage engines is ideally parallel to the X_m axis when the engine is in the null position. However, an engine's thrust vector alignment may deviate because of electrical and mechanical tolerances. To simulate the effect of the thrust vector deviation, the null position of each engine is assumed to be offset by the two small angles $\Delta\beta_{pi}$ and $\Delta\beta_{yi}$, for $i = 1, 2, 3, 4, 5$. Here, $\Delta\beta_{pi}$ and $\Delta\beta_{yi}$ have the same sense as β_p and β_y in Figure 1.

The method used to resolve the components of force of an S-IC stage engine along the vehicle axis is shown in Figure 14. In this figure, the (X'', Y'', Z'') triad has the same orientation as the (X_m, Y_m, Z_m) triad. $\overline{F}_{ei}$ is the thrust vector of engine i for $i = 1, 2, 3, 4, 5$. Note that $\beta_{p5} = \beta_{y5} = 0$ since the center engine does not gimbal (Figure 1). Let F_{exi},

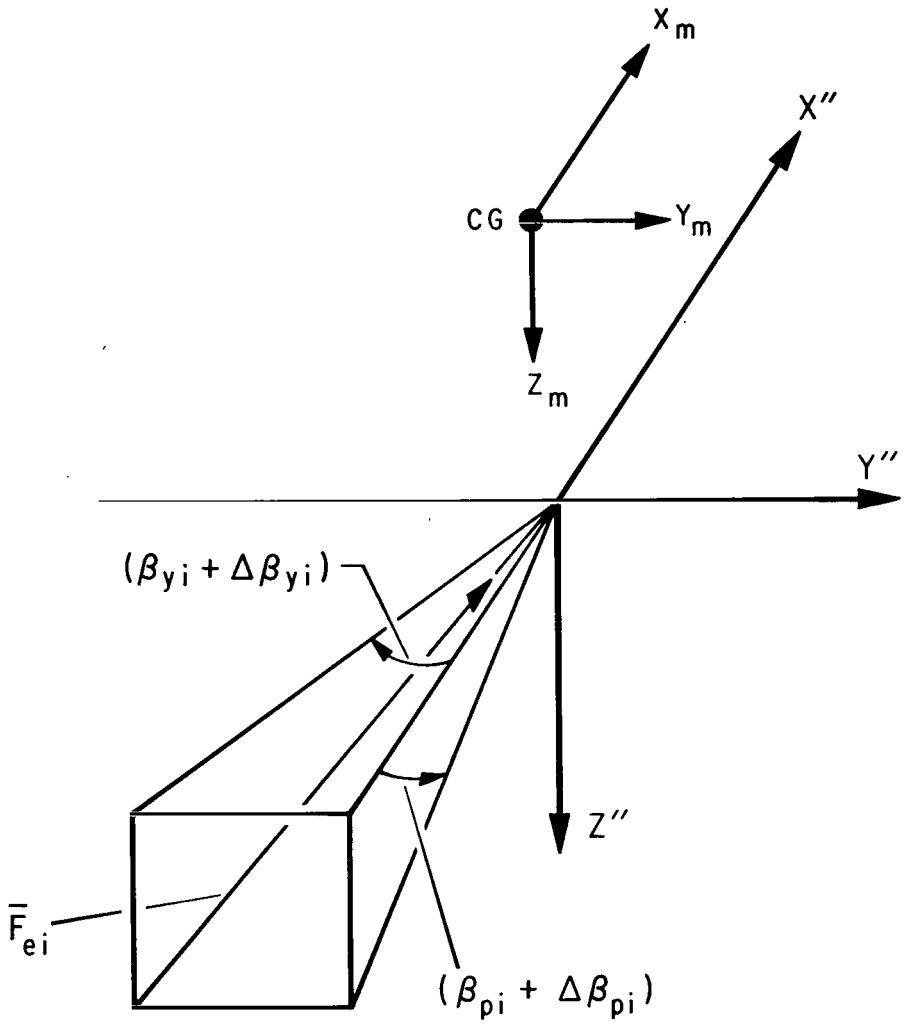

FIG. 14. RESOLUTION OF ENGINE FORCES

F_{eyi}, and F_{ezi} be the components of $\bar{F}_{ei}$ along the X", Y", Z" axes, respectively. From an inspection of Figure 14, it is easy to show that

$$F_{exi} = |\bar{F}_{ei}|/K \tag{4-19}$$

$$F_{eyi} = |\bar{F}_{ei}| \tan (\beta_{yi} + \Delta\beta_{yi})/K \tag{4-20}$$

and

$$F_{ezi} = - |\bar{F}_{ei}| \tan (\beta_{pi} + \Delta\beta_{pi})/K \tag{4-21}$$

where

$$K = \sqrt{1 + \tan^2 (\beta_{pi} + \Delta\beta_{pi}) + \tan^2 (\beta_{yi} + \Delta\beta_{yi})} \quad .$$

The thrust of each S-IC stage engine is a function of time and atmospheric pressure at the engine. $|\bar{F}_{ei}|$ is computed from the expression

$$|\bar{F}_{ei}| = F_{vi} - P_A A_i \quad , \tag{4-22}$$

where F_{vi} is the thrust of engine i firing in a vacuum, P_A is the atmospheric pressure at the engine, and A_i is the exit area of engine i . F_{vi} is predicted as a function of time.

As the vehicle's engines consume propellant, the vehicle CG and thus the origin of the (X_m, Y_m, Z_m) triad change with respect to the vehicle frame. A frame-fixed triad (X_f, Y_f, Z_f) is defined to serve as a reference for referring the location of the CG, the attach points of the engines, and

certain aerodynamic characteristics. The origin of this triad is at the intersection of the geometrical centerline of the vehicle and the plane that contains the attach points of the S-IC stage engines. The $+X_f$ axis is directed along the stage centerline, and the Y_f and Z_f axes are parallel to the Y_m and Z_m axes, respectively. Thus, this is a right-hand triad with the same orientation as the (X_m, Y_m, Z_m) triad (Figure 15).

An expression for the moment of an S-IC engine about the vehicle CG can now be derived. The total thrust of an engine is assumed to be applied at the attach point of the engine to the stage. Figure 15 shows the relative position of the vehicle CG with respect to the attach point of engine i. By definition, the moment $\overline{M}$ of a vector $\overline{V}$ about a point 0 is

$$\overline{M} = \bar{r} \times \overline{V} \quad , \tag{4-23}$$

where $\bar{r}$ is the vector directed from point 0 to the point of application of $\overline{V}$. Therefore, from Figure 15, the moment $\overline{M}_i$ of the thrust of engine i about the vehicle CG is

$$\overline{M}_i = \bar{r}_i \times \overline{F}_{ei} = (\overline{P}_i - \overline{CG}) \times \overline{F}_{ei} \quad , \tag{4-24}$$

where $\overline{P}_i$ and $\overline{CG}$ are the frame-fixed position vectors of the attach point of engine i and the vehicle CG, respectively.

The above equation along with equations (4-19), (4-20), and (4-21) provide the total model with expressions for computing the forces and moments resulting from the thrust of the S-IC stage engines.

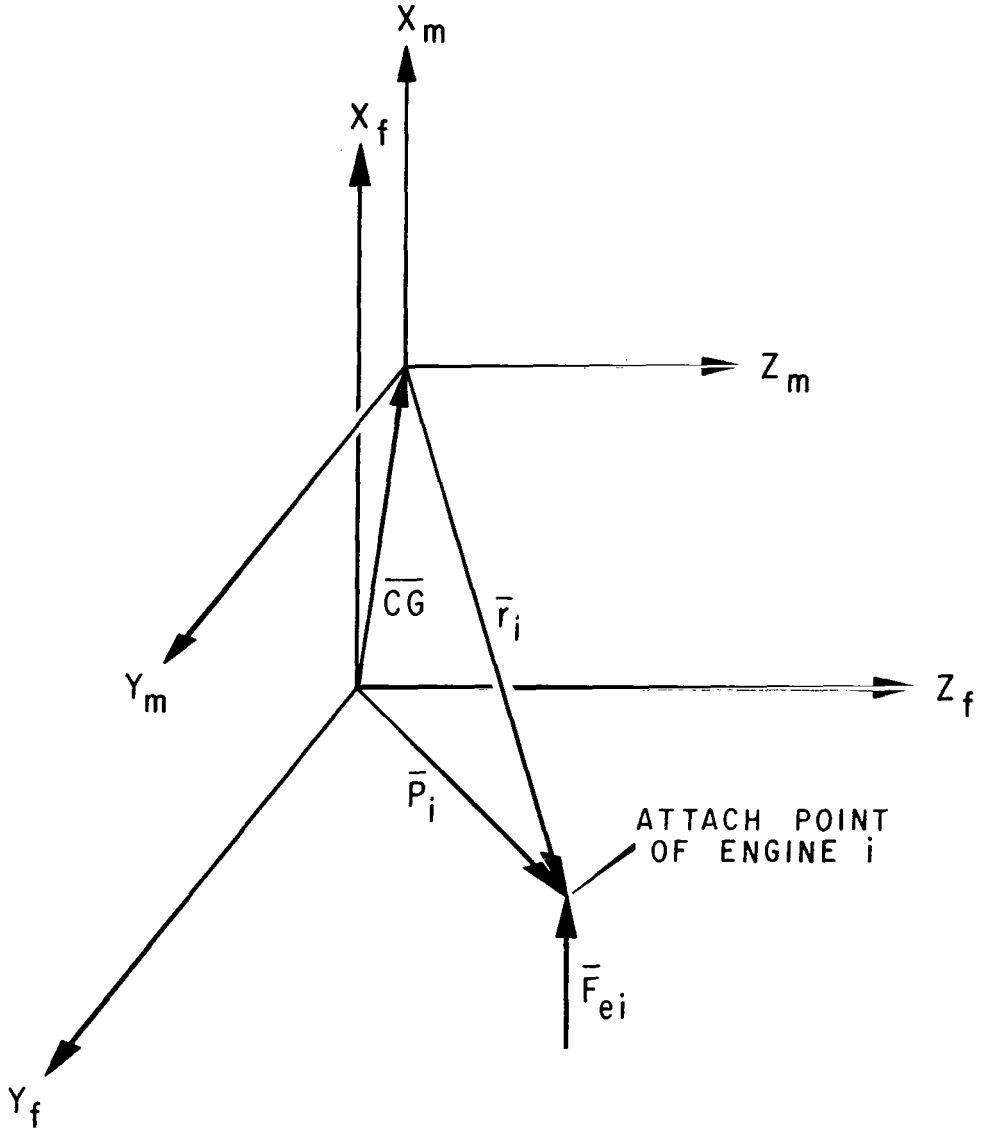

FIG. 15. FRAME-FIXED COORDINATE SYSTEM

A Newtonian potential function (Reference 1) is used to determine the earth's gravitational acceleration vector at the vehicle CG. This function was discussed briefly in Chapter I. No further discussion of this function will be presented here except to say that it uses the position vector, $\overline{PP}_u$, of the vehicle CG referred to the (U, V, W) equatorial triad to compute the gravitational acceleration of the vehicle.

The position vector $\overline{PP}_u$ will be computed from the vector $\overline{PP}_c$ (position of the vehicle CG relative to the earth-centered triad). From Figures 9 and 11,

$$\overline{PP}_c = \overline{R}(t=0)_s + \overline{RS}_s \quad . \tag{4-25}$$

Then by equation (2-3)

$$\overline{PP}_u = \left[\varphi_o - \pi/2\right]_y \left[A_z\right]_x \overline{PP}_c$$

$$= \left[\varphi_o - \pi/2\right]_y \left[A_z\right]_x \left(\overline{R}(t=0)_s + \overline{RS}_s\right) \quad . \tag{4-26}$$

$\overline{PP}_u$ is used as the independent variable in the Newtonian potential function to obtain the gravitational acceleration of the vehicle, $\overline{GR}_u$.

Since the equations of motion refer all translational motion of a vehicle to the surface triad, it is convenient to refer the gravitational acceleration to it also. Thus, by equation (2-2)

$$\overline{GR}_s = \left[A_z\right]_x^T \left[\varphi_o - \pi/2\right]_y^T \overline{GR}_u \quad . \tag{4-27}$$

The gravitational force vector, $\overline{FG}_s$, referred to the surface triad, can now be derived from an application of equation (3-7), the first law of motion of Newtonian Mechanics. Hence,

$$\overline{FG}_s = m\,\overline{GR}_s \tag{4-28}$$

where m is the mass of the vehicle.

As a vehicle flies through the earth's atmosphere, it experiences the forces of buoyance and air friction. The buoyance force, $\bar{F}_b$, is assumed to have the same direction as the position vector of the vehicle relative to the center of the earth. Its magnitude is

$$|\bar{F}_b| = V_A\,\rho\,|\overline{GR}_s| \quad , \tag{4-29}$$

where V_A is the volume of air displaced by the vehicle and ρ is the density of the air through which the vehicle is flying. Therefore,

$$\left(\bar{F}_b\right)_s = V_A\,\rho\,|\overline{GR}_s|\,\overline{PP}_c/|\overline{PP}_c| \quad . \tag{4-30}$$

Notice that $\overline{PP}_c/|\overline{PP}_c|$ is a unit vector that has the same direction as $\bar{F}_b$.

The point of application of $\bar{F}_b$ is assumed to be at the vehicle's CG. Therefore, the moment of $\bar{F}_b$ about the CG is zero.

Figure 16 shows a vehicle moving through the earth's atmosphere with velocity $\overline{RV}$ with respect to the surrounding air. Contact of the vehicle with particles of air produces a distribution of pressure over the vehicle's entire surface. Rather than consider the pressure distribution, its effect on the

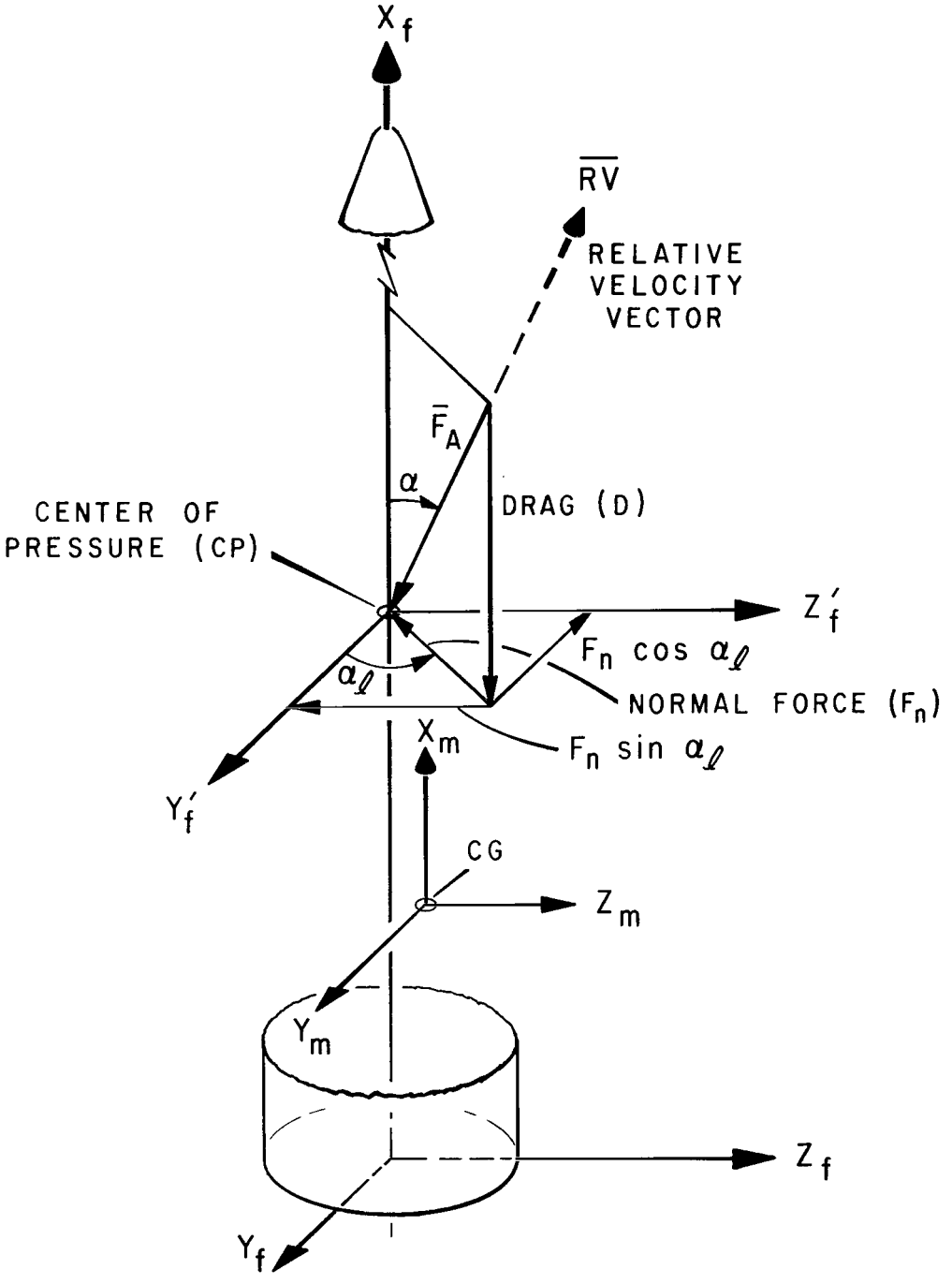

FIG. 16. AERODYNAMIC FORCES

motion of the vehicle is accounted for by applying a suitable single force at a point on the vehicle's geometric centerline called the center of pressure (CP). To preserve the laws of Newtonian mechanics, the single force, $\bar{F}_A$, must be equal to the vector sum of the forces of the pressure distribution, and the CP must be located at a point that causes the moment of $\bar{F}_A$ about the vehicle CG to equal the moment of the pressure distribution about the CG. Since the pressure distribution directly opposes the vehicle's relative velocity, $\bar{F}_A$ has the same sense as that of $-\overline{RV}$.

The total force, $\bar{F}_A$, is customarily resolved into two components. The normal force, F_n, is the component normal to the vehicle's longitudinal axis and the drag, D, is the component parallel to the longitudinal axis. Thus, to describe the aerodynamic force of the pressure distribution, the variation of F_n, D, CP, α, α_ℓ and $\overline{RV}$ must be specified.

For a given Mach number and α (angle-of-attack), F_n and D are proportional to the aerodynamic pressure, Q, and the cross-sectional area of the missile, A. Here,

$$\text{Mach} = |\overline{RV}|/VS \quad , \tag{4-31}$$

where VS is the velocity of sound in the air surrounding the vehicle and

$$Q = \rho\, |\overline{RV}|^2/2 \quad . \tag{4-32}$$

Because of these proportionalities, it is customary to write

$$F_n = C_n\, Q\, A \tag{4-33}$$

and

$$D = C_d Q A \tag{4-34}$$

where C_n and C_d are dimensionless proportionality coefficients.

Both coefficients and the distance from the origin of the (X_f, Y_f, Z_f) triad to the CP are determined experimentally as functions of Mach and α. Resolution of $\overline{F}_A$ into drag and normal force and the moment of $\overline{F}_A$ about the CG are directly dependent upon α. Dependence on Mach accounts for variation of these three parameters with air temperature as well as relative velocity. The main variation in the velocity of sound arises from the fact that the velocity is proportional to the square root of the absolute temperature.

$\overline{RV}$ is the difference between the velocity of the vehicle and the velocity of the air surrounding the vehicle. Since the earth's atmosphere rotates with the earth, the velocity of air has a component because of the rotation of the earth, $\left(\overline{\omega}_e\right)_s \times \overline{PP}_c$, and a second component because of the velocity of the air with respect to the earth, $\overline{W}_e$. Thus, $\overline{RV}$ referred to the (X_m, Y_m, Z_m) triad is

$$\overline{RV}_m = [TSM]\left\{ \dot{\overline{RS}}_s - \left(\overline{\omega}_e\right)_s \times \overline{PP}_c - [TSE]^T \overline{W}_e \right\} . \tag{4-35}$$

The parameters α and α_ℓ (Figure 16) are determined from the components of $\overline{RV}_m$. The expressions used for computing them are

$$\alpha = \arccos\left(\frac{RV_x}{|\overline{RV}_m|}\right) \tag{4-36}$$

and

$$\alpha_\ell = \arctan\left(\frac{RV_z}{RV_y}\right) \quad , \tag{4-37}$$

where RV_x, RV_y and RV_z are the components of $\overline{RV}_m$ along the X_m, Y_m, Z_m axes, respectively.

Expressions for the components of $\bar{F}_A$ along the vehicle-fixed axes can now be established. From Figure 16, it is easy to see that

$$\left(\bar{F}_A\right)_m = \begin{bmatrix} -D \\ -F_n \sin\alpha_\ell \\ -F_n \cos\alpha_\ell \end{bmatrix}_m \quad , \tag{4-38}$$

where D and F_n are defined by equations (4-33) and (4-34).

Equation (4-23) is used to determine an expression for the moment of $\bar{F}_A$ about the vehicle CG. From Figures 15 and 16, it is apparent that

$$\bar{r}_m = \begin{bmatrix} CP \\ 0 \\ 0 \end{bmatrix}_m - \overline{CG}_m \tag{4-39}$$

where $\bar{r}_m$ corresponds to $\bar{r}$ in equation (4-23) and CP is the distance from the origin of the (X_f, Y_f, Z_f) triad to the CP. Therefore, the aerodynamic moment, $\overline{M}_A$, of $\bar{F}_A$ about the CG is

$$\left(\overline{M}_A\right)_m = \bar{r}_m \times \left(\bar{F}_A\right)_m \quad . \tag{4-40}$$

Since the atmospheric parameters ρ, air density, P_A, atmospheric pressure, and VS, the velocity of sound, are functions of the altitude of the vehicle above the earth, an expression for altitude must be derived. Figure 17 shows a meridian through the polar axis of the earth that contains the position vector, $\overline{PP}_c$, of the vehicle CG with respect to the (X_c, Y_c, Z_c) triad. The following expressions are obvious from an inspection of the figure.

$$\theta = \arcsin\left(\frac{\overline{PP}_c}{|\overline{PP}_c|} \cdot \frac{(\overline{\omega}_e)_s}{|\overline{\omega}_e|}\right) \tag{4-41}$$

$$c = a\sqrt{\cos^2\theta + \left(\frac{a}{b}\sin\theta\right)^2} \tag{4-42}$$

$$h' = |\overline{PP}_c| - c \tag{4-43}$$

The variable h' in equation (4-43) is assumed to be a close approximation to the actual altitude h.

Expressions have now been developed for all forces and moments that a vehicle experiences as it moves through the earth's atmosphere. Thus, expressions for the total force and moment vectors can now be obtained by algebraically combining the individual contributors.

The total force is composed of the thrust of the five S-IC stage engines, the force of gravity, the buoyance force, and the aerodynamic force. Thus, the equation for the total force $\overline{F}_s$ is

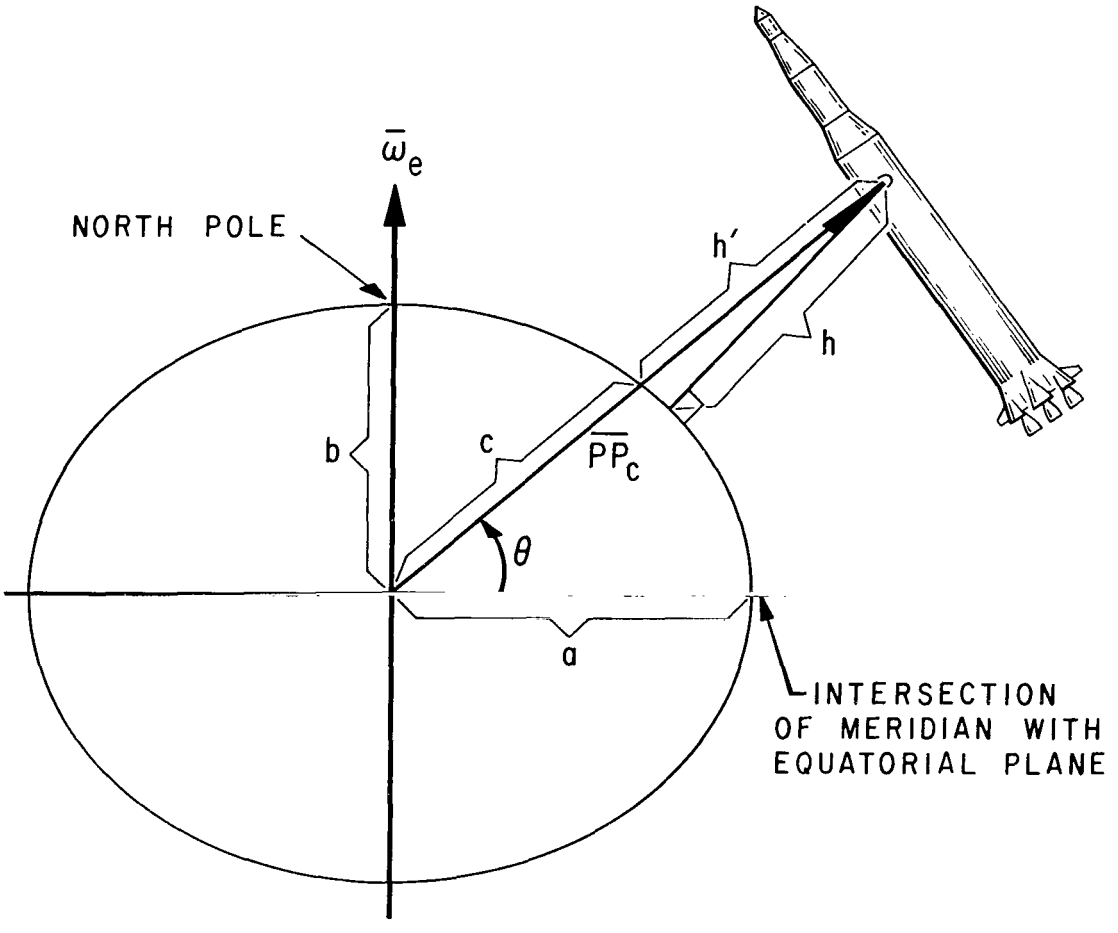

$$h \approx h'$$

$$|\overline{PP_c}| = c + h'$$

a - EQUATORIAL RADIUS OF EARTH

b - POLAR RADIUS OF EARTH

FIG. 17. ALTITUDE OF VEHICLE

$$\bar{F}_s = [TSM]^T \left(\sum_{i=1}^{5} \bar{F}_{ei} \right) + \overline{FG}_s + \left(\bar{F}_b \right)_s + [TSM]^T \left(F_A \right)_m \quad . . \tag{4-44}$$

The total moment about the vehicle CG is composed of the moments resulting from the five S-IC stage engines and the aerodynamic force. Therefore, the expression for the total moment vector, $\bar{M}_m$, is

$$\bar{M}_m = \left(\sum_{i=1}^{5} \bar{M}_i \right) + \left(\bar{M}_A \right)_m \quad . \tag{4-45}$$

CHAPTER V

NUMERICAL INTEGRATION

The design of a complex and expensive vehicle system such as the Saturn V requires an analysis of the response of a vehicle to different designs, vehicle engineering tolerances, and various atmospheric conditions. Because a large part of the analysis does not involve flexible motion of a vehicle, the rigid-body response can be predicted by electronic computer programs based on mathematical models like the one developed in this paper. Programs of this type require an efficient numerical integration technique that will provide a solution within the accuracy of the data which describe the vehicle dynamic response characteristics. One such program, the liftoff program, was developed from the mathematical model presented in Chapters II, III, and IV.

In a search for the most acceptable integration technique, the fourth-order Runge-Kutta formula and two of Dr. E. B. Shanks' integration formulas were each used in the liftoff program to compute the first stage trajectory of a typical Saturn V vehicle. Comparative data were generated for each formula over a range of integration step-sizes. Also, comparative data were

established for a technique associated with one of Dr. Shanks' formulas that regulates the integration step-size. An analysis of these data and a description of the integration formulas are presented in this chapter.

The three numerical integration techniques to be compared are the fourth-order Runge-Kutta formula, the fourth-order formula developed on page 8 of Reference 5, which shall be referred to as formula 4-3, and the fifth-order formula 5-5 presented in Reference 6. Only a description of the equations as they apply to a differential equation of the form $y' = \frac{dy}{dt} = f(t, y)$ need be given since the system of first and second order differential equations presented in Chapter III are reducible to an application of this result.

The Runge-Kutta formula is presented first. If the initial values of the differential equation $y' = f(t, y)$ are t_0, y_0, the value of y at $t_0 + h$ is computed from the formulas

$$
\begin{aligned}
f_0 &= f(t_0, y_0) \\
f_1 &= f\left(t_0 + \frac{h}{2}, y_0 + \frac{h f_0}{2}\right) \\
f_2 &= f\left(t_0 + \frac{h}{2}, y_0 + \frac{h f_1}{2}\right) \\
f_3 &= f(t_0 + h, y_0 + h f_2) \\
y &= y_0 + \frac{h}{6}(f_0 + 2f_1 + 2f_2 + f_3)
\end{aligned}
\qquad (5\text{-}1)
$$

evaluated in the given order. A derivation of this technique is given in most books on numerical analysis.

The formula 5-5 expressions for determining the value of y at $t_0 + h$ are

$$
\begin{aligned}
f_0 &= f(t_0 , y_0) \\
f_1 &= f(t_0 + h/9000 , y_0 + hf_0/9000) \\
f_2 &= f(t_0 + 3h/10 , y_0 - 404.7hf_0 + 405hf_1) \\
f_3 &= f(t_0 + 3h/4 , y_0 + 20241hf_0/8 - 20250hf_1/8 + 15hf_2/8) \\
f_4 &= f(t_0 + h , y_0 - 931041hf_0/81 + 931500hf_1/81 \\
&\qquad - 490hf_2/81 + 112hf_3/81)
\end{aligned}
\qquad (5\text{-}2)
$$

$$
y = y_0 + \frac{h}{1134} (105f_0 + 500f_2 + 448f_3 + 81f_4) ,
$$

where each formula is evaluated in the given order.

Formula 4-3 differs from the above formulas in that it uses $f[t_0 - h , y(t_0 - h)]$, the value of f at $t_0 - h$, in computing y. The value of y at $t_0 + h$ is determined from the expressions

$$
\begin{aligned}
f_0 &= f(t_0 , y_0) \\
f_1 &= f[t_0 - h , y(t_0 - h)] \\
f_2 &= f[t_0 + h/2 , y_0 + h(5f_0 - f_1)/8] \\
f_3 &= f[t_0 + h , y_0 + h(-3f_0 + f_1 + 4f_2)/2] \\
y &= y_0 + h(f_0 + 4f_2 + f_3)/6
\end{aligned}
\qquad (5\text{-}3)
$$

The fourth-order Runge-Kutta formula is used for the first integration step, then formula 4-3 is used to continue the integration process.

A method of controlling the integration step-size to obtain the required accuracy is presented in Reference 7. A method is introduced for computing an estimate of the integration error made at each step. The error estimate, called a regulator, is used to determine the step-size for the next integration step.

The regulator for formula 4-3 is given in Reference 5. By combining the f_i of equation (5-3) by the formula

$$y_1 = y_0 + h(-5f_0 + f_1 + 12f_2 - 2f_3)/6 \quad , \qquad (5\text{-}4)$$

a third-order solution for y at $t_0 + h$ is obtained. The regulator, R, is defined to be the absolute value of the difference between the values of y computed from equations (5-3) and (5-4); that is,

$$R = |y - y_1| = \frac{h}{6} |6f_0 - f_1 - 8f_2 + 3f_3| \quad . \qquad (5\text{-}5)$$

Thus, R is a fourth-order estimate of the third-order error. Note that the number of additional calculations required to compute R are insignificant since the same evaluations of f are used to compute both y and R.

When the integration process extends over a number of steps, the value of R can be monitored and used as an error indicator for controlling the step-size. To accomplish this, a lower limit L_1 and an upper limit L_2 $(0 < L_1 < L_2)$ are established for R. At the end of each integration step, R is compared

with these limits. If $R < L_1$, the step-size is doubled; if $R > L_2$, the step-size is halved; if $L_1 \leq R \leq L_2$, the step-size is not changed. When the step-size is changed, the fourth-order Runge-Kutta formula is used over the next step to establish a value for f_1 in equation (5-3). The integration process is then continued with formula 4-3.

The differential equations of the liftoff program reduce to a system of twelve first order differential equations. Thus, twelve distinct values of R can be calculated at the end of each integration step. Which of the twelve values of R or what combination of the twelve values of R should be monitored for controlling the integration step-size is an important question that must be answered in order to effectively use this procedure in the liftoff program. This question can be answered by determining which distinct values of R are most sensitive to the total accuracy of formula 4-3 in integrating the equations of motion. The data required to obtain this information can be described more easily after the comparative data for the three integration routines are presented.

Before the comparative data were generated, a computer program was written and verified for each of the three integration formulas. The programs were written for the SDS-930 computer at Marshall Space Flight Center in Huntsville, Alabama. The differential equation $x^2y'' + 2xy' + 2y + 4 + x = 0$ which has $y = c_1x + c_2/x^2 - 2 + x^2/4$ as a general solution was chosen to be used in verifying the programs. Choosing $x = 1$, $y = 1/4$, and $y' = -25/8$ as initial values, the exact solution for $x \neq 0$ becomes $y = x/8 + 15/8x^2 + x^2/4$.

This equation was then numerically integrated over the interval $x = .1$ to $x = 5$ to obtain the following data.

Runge-Kutta 4-4		Formula 4-3		Formula 5-5	
Step-Size	Error	Step-Size	Error	Step-Size	Error
.10	$.10 \times 10^{4}$	.10	$.11 \times 10^{4}$	.10	$.10 \times 10^{3}$
.05	$.95 \times 10^{2}$	.05	$.10 \times 10^{3}$	.05	$.46 \times 10^{1}$
.025	$.65 \times 10^{1}$	.025	$.61 \times 10^{1}$	.025	$.15 \times 10^{0}$
.01	$.16 \times 10^{0}$	.01	$.53 \times 10^{-1}$	.01	$.15 \times 10^{-2}$
.005	$.10 \times 10^{-1}$	.005	$.32 \times 10^{-1}$	.005	$.48 \times 10^{-4}$
.0025	$.62 \times 10^{-3}$	.0025	$.60 \times 10^{-2}$	.0025	$.28 \times 10^{-5}$
.001	$.16 \times 10^{-4}$	.001	$.46 \times 10^{-3}$	.001	$.12 \times 10^{-5}$
.0005	$.30 \times 10^{-5}$	.0005	$.59 \times 10^{-4}$		

Next, the trajectory parameters to be analyzed for comparing the different integration formulas in the liftoff program had to be selected. A time history of the vehicle position and orientation with respect to the (X_s, Y_s, Z_s) triad basically defines the vehicle trajectory. For this reason, the parameters xs_p, ys_p, zs_p, φ_p, φ_y, and φ_r are the obvious ones to be contrasted.

Selection of data for use in generating the comparison results was the next task. Data which represent the dynamic characteristics of a typical Saturn V vehicle were chosen. Large dynamic disturbances were imposed on the trajectory by failing an S-IC stage outboard engine 70 seconds after liftoff and disturbing the atmosphere with a wind that peaked immediately following the engine failure (Figure 18). The wind was directed normal to the

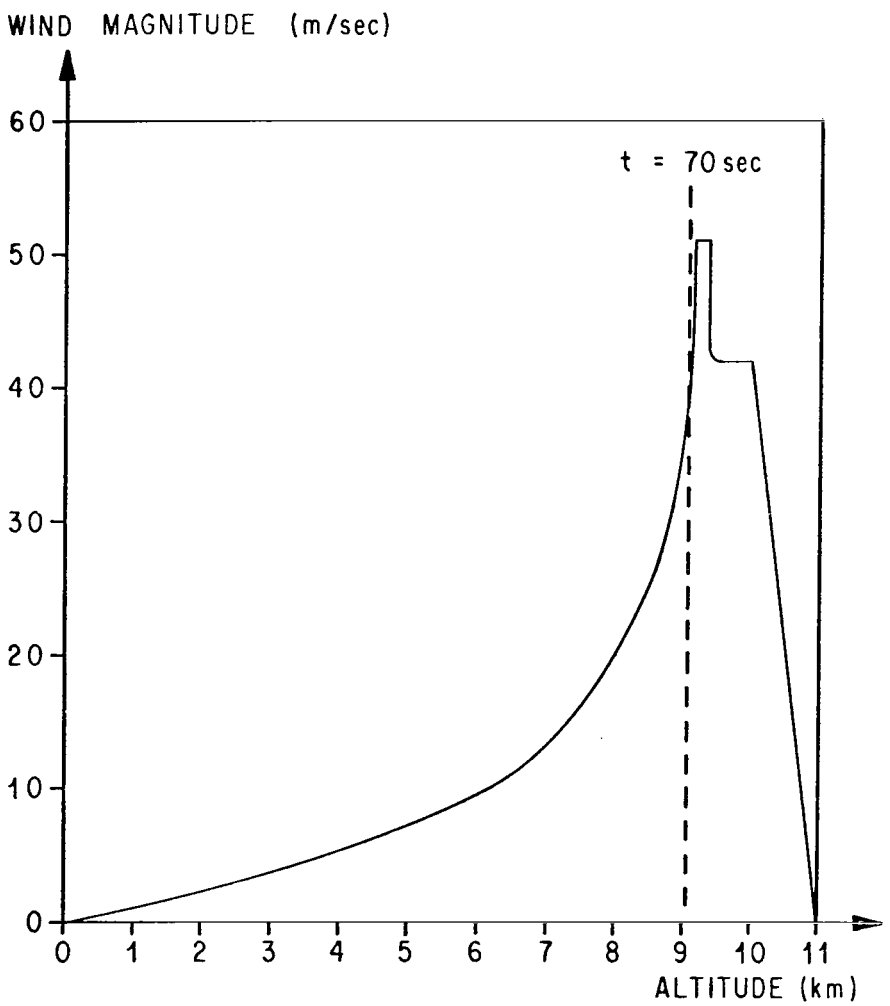

FIG. 18. WIND PROFILE

vehicle flight path in the direction that would create an aerodynamic moment on the vehicle having the same sense as the moment created by the engine failure. When the entire wind profile is increased by 1 meter-per-second, the control system is incapable of continuing to control the vehicle's attitude after the engine failure. That is, the aerodynamic moment forces the vehicle to begin to tumble. Thus, the chosen trajectory is representative of nominal flight before 70 seconds and highly disturbed flight thereafter.

The liftoff program is written in single-precision for a CDC-3200 computer at the Marshall Space Flight Center in Huntsville, Alabama. (Single-precision on this computer means that eleven digits other than the exponent are assigned to each floating point number.) Tables 1, 2, and 3 present comparative data obtained from this program for different integration formulas and step-sizes at the 70, 80, and 90 second time points of the trajectory. The three different time points in the trajectory are presented in case any one formula is biased at any one of the time points.

The data presented in the tables were obtained from an on-line printer while the trajectories were being computed. Since the CDC-3200 computer does not print and compute simultaneously, run time is affected by the amount of output obtained. For this reason, only a small amount of output was obtained from the trajectories for which the computation times are presented in Tables 1, 2, and 3. During the first 70 seconds of each trajectory, output was obtained every 10 seconds; for the remainder of the trajectory output was obtained every 5 seconds.

Some way of comparing the accuracy of the solutions presented in the tables must be established in order to evaluate the comparative data. At present, no means of determining an exact solution to a trajectory based on a specific set of vehicle dynamic data exist. A review of Tables 1, 2, and 3 reveals that the differences between the solutions reached by the three formulas are less than 1 percent in all parameters except the roll and yaw attitude angles which differ less than 4 and 6 percent, respectively, at the 90 second time point. Therefore, it shall be assumed that the exact solution does not differ more than these percentages from the solution reached by any one of the formulas. Based on this assumption, the accuracy of each formula can be judged by whether the difference between the solution it reached and the solutions reached by the other two formulas is within the accuracy of the data that describe the dynamic characteristics of the vehicle.

Because of hardware and engineering tolerances, the dynamic characteristics of a vehicle cannot be predicted exactly. Publications that present the dynamic data for a particular Saturn V vehicle give the statistical variations of the data. The one-sigma data tolerances are listed in Table 4. The effects of these tolerances on the trajectory when applied to the dynamic data used to generate Tables 1, 2, and 3 were assessed using formula 4-3 with an integration step-size of .125. Tables 5, 6, and 7 give the solution of the trajectory at 70, 80, and 90 seconds, respectively, with the specific tolerances applied in both the most helpful and most harmful way. Here, the most helpful way is defined to be an application of the tolerance that reduces the effect of the

engine failure and wind disturbances; the most harmful way is defined to be an application of the tolerance that increases the effect of the engine failure and wind disturbances. The effect of each tolerance can be assessed by comparing the formula 4-3 solution of Tables 1, 2, and 3 with Tables 5, 6, and 7.

A comparison of Tables 5, 6, and 7 with Tables 1, 2, and 3 shows that differences in the solutions reached by all three integration techniques are within the accuracy of the Saturn V dynamic data. Therefore, by this method of judging accuracy, all three integration techniques are acceptable from an accuracy stand point.

A study of Tables 1, 2, and 3 reveals that formula 4-3 would be the most desirable integration formula to use in the liftoff program from a standpoint of computer run time, accuracy, and stability of the solution. At all three time points, the three formulas reach a stable solution at the same step-size. Also, the solution reached by formula 4-3 does not differ significantly from the solutions reached by the other formulas, and this difference is within the accuracy of the input data. The differences between the Runge-Kutta solution and the formula 4-3 solution are so small that the solutions are, for all practical purposes, identical. This fact is important since the fourth-order Runge-Kutta formula is presently being used almost exclusively in all digital trajectory programs at Marshall Space Flight Center. Computer time would be saved by use of the formula 4-3 since it requires less computation time for a given step-size than the other two formulas.

As previously stated, the input data chosen for this study resulted in a trajectory that has both nominal and highly abnormal vehicle dynamics. The first 70 seconds of the trajectory represents normal dynamics since the vehicle is disturbed only by a wind. An engine failure in combination with the wind resulted in dynamics which very closely approached control loss following 70 seconds. Thus, the formula 4-3 has proven to be the most practical formula for integrating both nominal and highly off-nominal vehicle dynamics.

With the 4-3 formula established as a practical one to use in the liftoff program, an investigation of the value of the formula 4-3 regulator for controlling the step-size in the program becomes a logical extension of this analysis. As previously stated, twelve distinct values for the regulator can be obtained at each integration step in the liftoff program. Effective control of the step-size requires a regulator that is sensitive to the total accuracy of the integration process. Since all the parameters obtained by integration are related through the differential equations, the selected regulator must be a function of the regulators for the parameters that contain the largest percentages of integration error. Here, the percentage of integration error for a parameter is defined to be: $100 \times$ integration error $\div$ absolute magnitude of the parameter. By assuming a regulator to be a good approximation of the actual integration error, we can determine these parameters by analyzing the twelve regulator values for various integration step-sizes. Figures 19 through 30 present the time variations of the twelve difference regulators for integration step-sizes from .03125 to .50 . The Saturn V dynamic data used to generate Tables 1, 2, and 3 were also used to generate these figures.

Table 8 lists the twelve parameters that are integrated and gives the largest percentage of error associated with each one. The largest percentage of error for a parameter was computed by using the peak value of the parameter's regulator at a step-size of .50 as the maximum integration error. Table 8 indicates that the regulators for ω_x, ω_y, and ω_z are the ones most sensitive to the total accuracy of the integration process. A comparison of the regulators for these three parameters (Figures 25, 26, and 27) with the other nine regulators verifies this. That is, the response of these three regulators to the engine failure and wind gust disturbances at 70 seconds was much greater than the response of the other nine regulators.

With the regulators for ω_x, ω_y, and ω_z established as the ones most sensitive to the total integration accuracy, the question of how to combine them into one total regulator must now be answered. Figures 25, 26, and 27 show that the regulator for ω_x is approximately ten times larger than the regulators for ω_y and ω_z. This prevents the three regulators from being combined directly. Equation (3-33) shows that any disturbance that affects the roll attitude also affects the pitch and yaw attitude. (Notice that $\omega_x \approx d\varphi_r/dt$, $\omega_y \approx d\varphi_p/dt$, and $\omega_z \approx d\varphi_y/dt$.) Based on these two facts, the decision was made to use the root-sum-square of the regulator for ω_y and ω_z as the total regulator for controlling the step-size in the liftoff program. Figure 31 presents the time variation of the total regulator for step-sizes from .03125 to .50.

Limits must be established for this regulator in order to use it to control the integration step-size. These limits are used in combination with maximum and minimum restrictions on the step-size to maintain an acceptable integration error. The step-sizes required to obtain an acceptable solution can be determined from Tables 1, 2, and 3. From liftoff to 70 seconds, a step-size of .50 is acceptable; from 70 to 90 seconds a step-size between .125 and .25 is required. Thus, the maximum and minimum restrictions on the step-size would be .50 and .125, respectively. The upper limit, L_2, for the total regulator can be established from Figure 31. Before 70 seconds, the regulator for a step-size of .50 does not exceed .00025. Following 70 seconds, the regulator exceeds .00025 once for a step-size of .125 and twice for a step-size of .25. Therefore, L_2 was chosen to be .00025. An effective value for the lower limit, L_1, was established from a tabulation of the time variation of the total regulator with step-size. A value of .00005 was chosen for L_1 since this value would allow the step-size to increase only when the regulator began to reach a significant peak. These values for L_1 and L_2 were verified as being reasonable by a number of computer runs using small variations to these numbers. The Saturn V dynamic data used to generate Tables 1, 2, and 3 were also used in these verification runs. Since the above regulator and step-size limits were established for a trajectory that contains both nominal and highly disturbed dynamics, they should be valid for any trajectory required by a vehicle design or design assurance study.

The formula 4-3 routine for the liftoff program was modified to use the total regulator, R, for controlling the step-size. If $R < L_1$, the step-size is doubled; if $R > L_2$, the step-size is halved; if $L_1 \leq R \leq L_2$, the step-size is not changed. However, before the step-size is changed, the value to which the step-size is to be changed is checked to make sure it is not outside the step-size restrictions.

With $L_1 = .00005$, $L_2 = .00025$ and $.50$ and $.125$ as the maximum and minimum step-size, respectively, a trajectory was computed with the modified formula 4-3 routine. The solution of this trajectory at the 70, 80, and 90 second time points is presented by Table 9. This solution is not only more accurate than the formula 4-3 solution with a step-size of .25 (Tables 1, 2, and 3), it also required 25 percent less computer time. Thus, the chosen regulator has been shown to be an effective indicator for controlling the integration error and reducing the computer time.

This chapter has established that the fourth-order formula 4-3 is a practical integration formula to use in the liftoff program. Since this program contains the basic differential equations of motion of which most rigid-body trajectory programs are composed, the formula 4-3 numerical integration routine has been shown to be more practical to use in these programs than either the fourth-order Runge-Kutta formula or the fifth-order formula 5-5. In addition, the technique for controlling the integration step-size associated with the formula 4-3 has been shown to effectively increase the efficiency of the formula by as much as 25 percent when the trajectory being computed contains large dynamic disturbances.

Table 1. Solution of Trajectory at 70 Seconds

Step-Size	φ_p	φ_y	φ_r	xs_p	ys_p	zs_p	Time* (min)
			Formula 4-3				
.03125	-28.7873	-.4728	.0027	8947.70	11009.18	36465.81	23.646
.0625	-28.7873	-.4728	.0027	8947.69	11009.17	36465.80	12.066
.125	-28.7873	-.4725	.0027	8947.18	11009.17	36465.73	6.306
.25	-28.7873	-.4729	.0027	8947.88	11009.14	36465.72	3.321
.50	-28.7872	-.4717	.0027	8946.41	11009.13	36465.54	2.005
			Runge-Kutta Formula				
.03125	-28.7873	-.4726	.0027	8947.34	11009.19	36465.79	30.814
.0625	-28.7873	-.4726	.0027	8947.38	11009.18	36465.78	15.650
.125	-28.7873	-.4724	.0027	8947.15	11009.18	36465.72	8.075
.25	-28.7874	-.4727	.0027	8948.00	11009.14	36465.69	4.258
.50	-28.7873	-.4709	.0027	8946.41	11009.14	36465.43	2.432
			Formula 5-5				
.03125	-28.7876	-.4743	.0027	8950.43	11009.00	36465.65	42.697
.0625	-28.7876	-.4741	.0027	8950.10	11009.02	36465.75	21.431
.125	-28.7876	-.4740	.0027	8950.11	11009.06	36465.75	10.820
.25	-28.7875	-.4732	.0027	8949.16	11009.05	36465.65	5.663
.50	-28.7873	-.4719	.0027	8947.76	11008.96	36465.74	3.185

* Actual computer time used for computing the first 90 seconds of the trajectory. This number does not include time used in loading deck or reading data.

Table 2. Solution of Trajectory at 80 Seconds

Step-Size	φ_p	φ_y	φ_r	xs_p	ys_p	zs_p	Time* (min)
			Formula 4-3				
.03125	-38.7233	-16.5128	-12.4525	12180.78	12036.13	42546.21	23.646
.0625	-38.7237	-16.5187	-12.4552	12180.74	12036.11	42546.19	12.066
.125	-38.7233	-16.5169	-12.4545	12180.19	12036.18	42546.11	6.306
.25	-38.7158	-16.4344	-12.4212	12181.15	12036.22	42546.14	3.321
.50	-39.0284	-18.5710	-12.8615	12177.08	12031.53	42545.32	2.005
			Runge-Kutta Formula				
.03125	-38.7211	-16.5001	-12.4479	12180.36	12036.18	42546.18	30.814
.0625	-38.7266	-16.5366	-12.4628	12180.38	12036.11	42546.15	15.650
.125	-38.7215	-16.4964	-12.4460	12180.17	12036.24	42546.10	8.075
.25	-38.7129	-16.3931	-12.4018	12181.32	12036.36	42546.13	4.258
.50	-38.9201	-17.8007	-12.7405	12177.60	12032.99	42545.28	2.432
			Formula 5-5				
.03125	-38.6932	-16.2973	-12.3574	12184.00	12036.10	42546.09	42.697
.0625	-38.6962	-16.3158	-12.3661	12183.63	12036.12	42546.23	21.431
.125	-38.6922	-16.2869	-12.3540	12183.64	12036.23	42546.25	10.820
.25	-38.6869	-16.2431	-12.3358	12182.59	12036.48	42546.14	5.663
.50	-38.6550	-15.9663	-12.1963	12181.28	12037.31	42546.33	3.185

* Actual computer time used for computing the first 90 seconds of the trajectory. This number does not include the time used in loading the deck or reading data.

Table 3. Solution of Trajectory at 90 Seconds

Step-Size	φ_p	φ_y	φ_r	xs_p	ys_p	zs_p	Time* (min)
			Formula 4-3				
.03125	-44.9268	15.9817	7.6516	15575.30	12678.83	49598.65	23.646
.0625	-44.9276	16.0061	7.6691	15575.20	12678.51	49598.58	12.066
.125	-44.9273	15.9925	7.6596	15574.61	12678.68	49598.49	6.306
.25	-44.9169	15.6544	7.4057	15576.48	12682.91	49599.23	3.321
.50	-44.3560	19.4485	9.7651	15545.42	12518.26	49581.74	2.005
			Runge-Kutta Formula				
.03125	-44.9252	15.9302	7.6136	15574.95	12679.55	49598.69	30.814
.0625	-44.9300	16.0834	7.7227	15574.63	12677.58	49598.39	15.650
.125	-44.9254	15.9176	7.6010	15574.76	12679.82	49598.62	8.075
.25	-44.9133	15.5145	7.2618	15577.00	12685.16	49599.52	4.258
.50	-44.8984	20.0205	9.9560	15557.96	12592.42	49587.85	2.432
			Formula 5-5				
.03125	-44.8996	15.0857	6.8810	15580.62	12689.61	49600.12	42.697
.0625	-44.9021	15.1658	6.9562	15580.09	12688.74	49600.16	21.431
.125	-44.8990	15.0514	6.8434	15580.31	12690.27	49600.40	10.820
.25	-44.8951	14.8850	6.6719	15579.45	12692.71	49600.52	5.663
.50	-44.8646	13.8237	5.8255	15580.10	12706.29	49602.60	3.185

* Actual computer time used for computing the first 90 seconds of the trajectory. This number does not include the time used in loading the deck or reading data.

Table 4. One-Sigma Data Tolerances

Tolerance Number	Tolerance
1	.1 degree thrust vector misalignment of each S-IC stage engine in the same direction
2	.3 percent variation of the total thrust magnitude of the S-IC stage engines
3	2/3 inch lateral deviation of the predicted location of the missile center-of-gravity
4	2/3 meter variation of the predicted aerodynamic center-of-pressure
5	2 percent variation of the predicted aerodynamic normal force coefficient C_N
6	3.33 percent variation of the predicted aerodynamic drag coefficient C_d
7	2722 kilogram variation in the predicted initial mass of the missile

Table 5. Effects of One-Sigma Data Tolerances on Solution of Trajectory at 70 Seconds

Tolerance* Number	φ_p	φ_y	φ_r	xs_p	ys_p	zs_p
+1	-28.7017	-.3893	.0031	8949.35	11054.09	36401.81
-1	-28.8730	-.5559	.0022	8944.70	10964.07	36529.69
+2	-28.8044	-.5687	.0029	9062.40	11007.56	36479.13
-2	-28.7734	-.3990	.0033	8831.88	11010.71	36452.34
+3	-28.8178	-.4992	-.0347	8945.35	10974.86	36514.07
-3	-28.7569	-.4461	.0400	8948.84	11043.34	36417.43
+4	-28.7886	-.4015	.0032	8947.15	11013.52	36465.78
-4	-28.7860	-.5442	.0022	8947.22	11004.87	36465.68
+5	-28.7874	-.4647	.0027	8947.17	11010.91	36465.73
-5	-28.7871	-.4803	.0028	8947.20	11007.46	36465.73
+6	-28.7895	-.4849	.0027	8962.74	11008.95	36467.89
-6	-28.7852	-.4613	.0028	8933.03	11009.34	36463.56
+7	-28.7925	-.4997	.0026	8983.45	11008.58	36470.28
-7	-28.7824	-.4473	.0029	8910.99	11009.76	36461.20

* The tolerances are defined by Table 4. A positive tolerance number indicates that the tolerance was applied in the most helpful way; a negative tolerance number indicates that the tolerance was applied in the most harmful way.

Table 6. Effects of One-Sigma Data Tolerances on Solution of Trajectory at 80 Seconds

Tolerance* Number	φ_p	φ_y	φ_r	xs_p	ys_p	zs_p
+1	-38.3341	-14.9379	-11.5715	12184.76	12094.26	42468.09
-1	-39.1924	-18.3642	-12.5339	12175.13	11977.75	42624.17
+2	-38.4141	- 9.7470	- 6.2857	12334.38	12040.72	42573.47
-2	-40.1522	-26.3994	-13.3281	12025.63	12032.69	42518.46
+3	-38.6592	-16.1072	-12.4730	12177.77	11994.18	42604.66
-3	-38.8017	-16.9819	-12.3504	12182.35	12077.95	42487.61
+4	-38.1799	- 9.4252	- 5.8506	12185.03	12057.55	42546.86
-4	-41.5404	-32.0683	-13.3339	12172.33	12010.78	42544.29
+5	-38.3416	-13.8243	-10.6210	12181.95	12043.89	42546.19
-5	-39.3255	-20.0300	-12.8337	12178.20	12028.17	42545.95
+6	-38.5942	-15.3986	-11.9084	12203.54	12036.76	42551.62
-6	-38.7556	-16.9253	-12.6127	12159.15	12037.06	42540.83
+7	-38.4446	-14.0336	-10.8898	12229.68	12037.04	42555.64
-7	-39.0920	-19.2638	-12.8763	12130.81	12035.54	42536.59

* The tolerances are defined by Table 4. A positive tolerance number indicates that the tolerance was applied in the most helpful way; a negative tolerance number indicates that the tolerance was applied in the most harmful way.

Table 7. Effects of One-Sigma Data Tolerances on Solution of Trajectory at 90 Seconds

Tolerance* Number	φ_p	φ_y	φ_r	xs_p	ys_p	zs_p
+1	-44.7510	10.3892	4.7007	15592.16	12816.49	49514.55
-1	-44.2339	18.2383	9.0583	15543.26	12455.62	49678.34
+2	-44.1665	2.7922	.9414	15798.29	12862.91	49682.44
-2	-42.7376	-37.5092	-407.550	14636.99	12306.83	48931.55
+3	-44.9339	14.5655	6.7857	15574.91	12647.18	49699.56
-3	-44.9066	17.6410	8.1382	15573.06	12704.55	49526.97
+4	-44.1551	1.9187	.5546	15614.33	12890.09	49635.84
-4	-50.6667	-46.7982	-466.011	14696.97	12333.00	48871.73
+5	-44.6586	8.0330	3.5145	15593.61	12787.78	49614.93
-5	-209.788	-17.8573	-289.193	15343.07	12191.16	49450.16
+6	-44.8128	11.8636	5.6754	15614.90	12727.34	49616.93
-6	-44.9548	17.4259	8.4833	15541.61	12659.01	49584.86
+7	-44.6642	8.8958	3.9456	15652.43	12771.53	49630.58
-7	-42.6074	10.6717	5.3222	15463.93	12418.64	49556.72

* The tolerances are defined by Table 4. A positive tolerance number indicates that the tolerance was applied in the most helpful way; a negative tolerance number indicates that the tolerance was applied in the most harmful way.

Table 8. Integration Error Percentages

Parameter	Maximum Percentage of Integration Error
XSp	$.38 \times 10^{-2}$
dX_s/dt	$.12 \times 10^{0}$
YSp	$.29 \times 10^{-2}$
dY_s/dt	$.22 \times 10^{0}$
ZSp	$.12 \times 10^{-2}$
dZ_s/dt	$.28 \times 10^{0}$
ω_x	$.43 \times 10^{1}$
ω_y	$.19 \times 10^{1}$
ω_z	$.20 \times 10^{1}$
φ_p	$.93 \times 10^{-2}$
φ_y	$.77 \times 10^{0}$
φ_r	$.82 \times 10^{0}$

Table 9. Formula 4-3 Solution of Trajectory with Variable Step-Size

Trajectory Time (sec)	φ_p	φ_y	φ_r	XS_p	YS_p	ZS_p	Computer Time (min)
70	-28.7874	- .4726	.0027	8947.90	11009.12	36465.63	
80	-38.7193	-16.4557	-12.4490	12181.17	12036.17	42546.04	
90	-44.9181	15.7993	7.5117	15576.26	12681.74	49598.98	2.466*

* Actual computer time used for computing the first 90 seconds of the trajectory. This number does not include time used in loading deck or reading data.

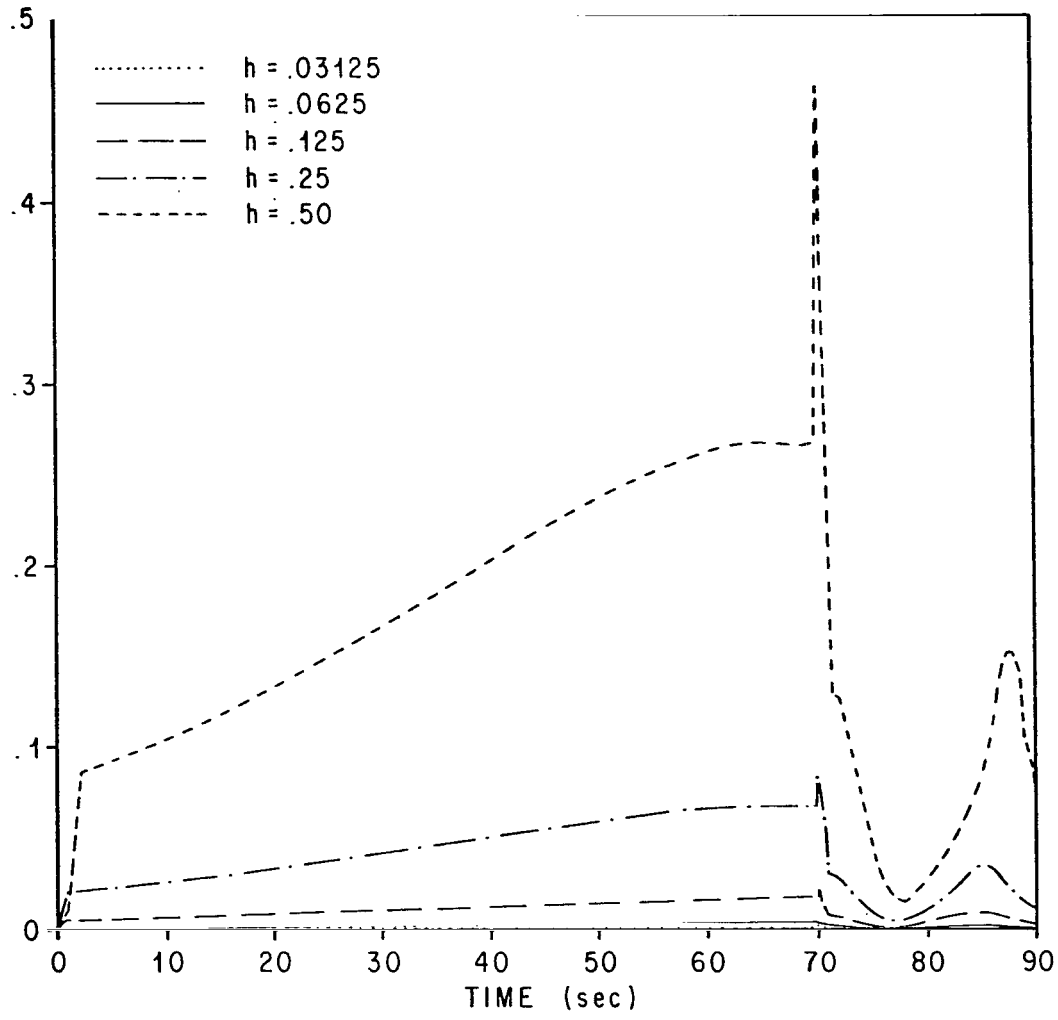

FIG. 19. REGULATOR FOR $XS_p = \int_{t_n}^{t_n+h} \left(\frac{dX_s}{dt}\right) dt$

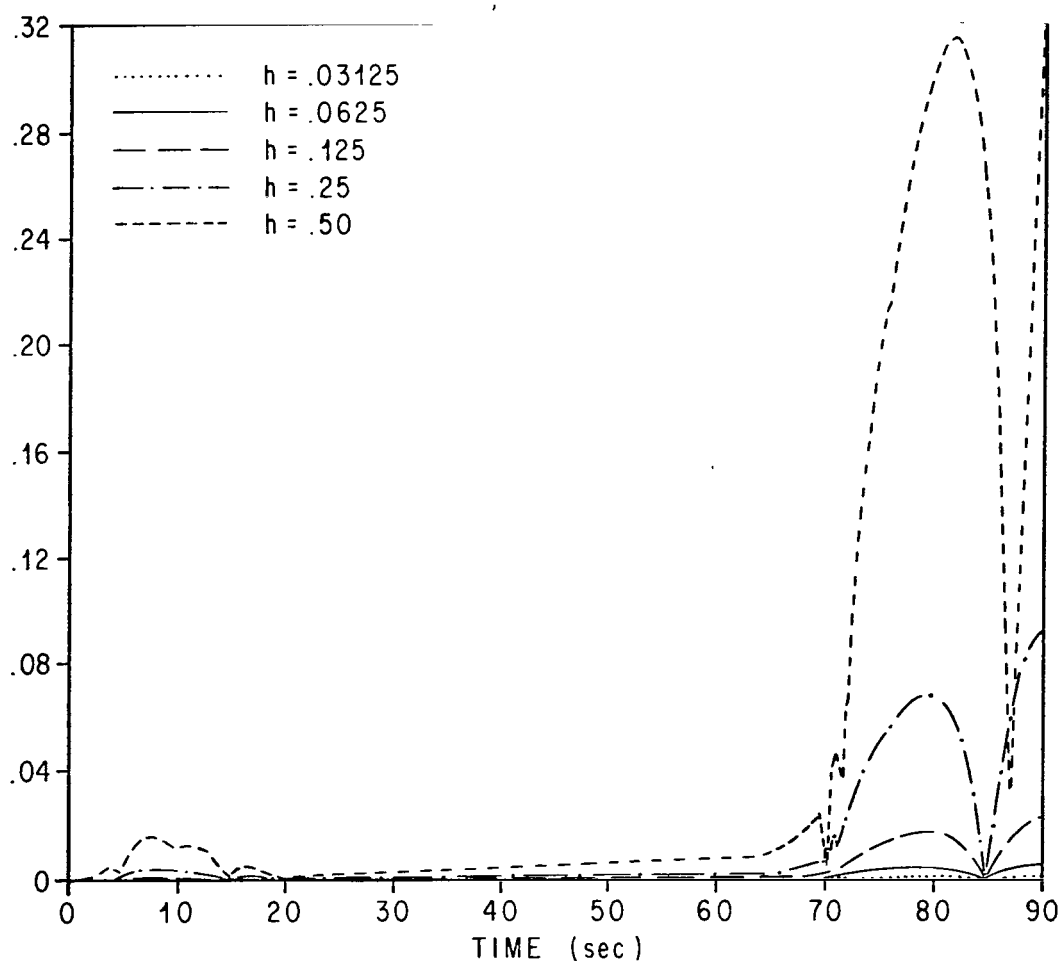

FIG. 20. REGULATOR FOR $YS_p = \int_{t_n}^{t_n+h} \left(\frac{dY_s}{dt}\right) dt$

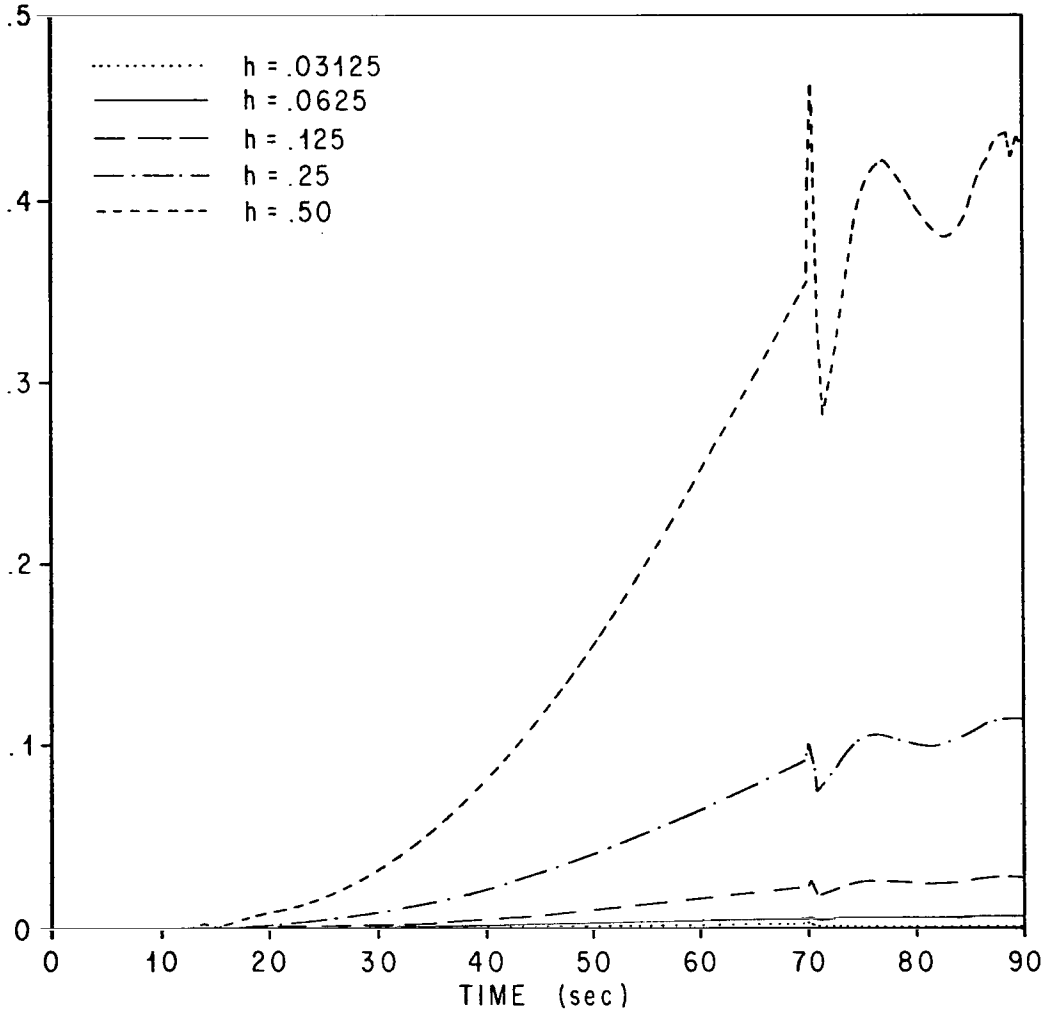

FIG. 21. REGULATOR FOR $ZS_p = \int_{t_n}^{t_n+h} \left(\frac{dZ_s}{dt}\right) dt$

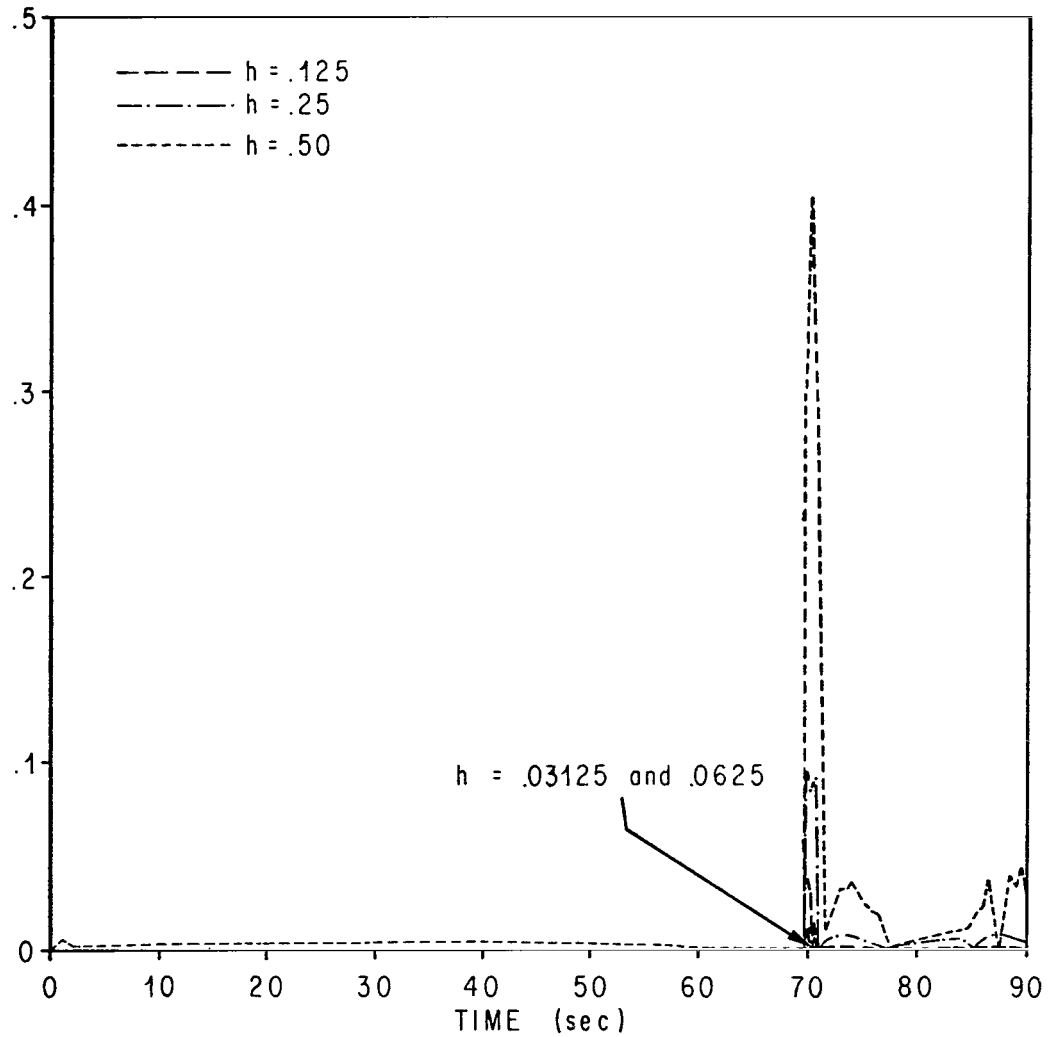

FIG. 22. REGULATOR FOR $\left(\frac{dX_s}{dt}\right) = \int_{t_n}^{t_n+h} \left(\frac{d^2X_s}{dt^2}\right) dt$

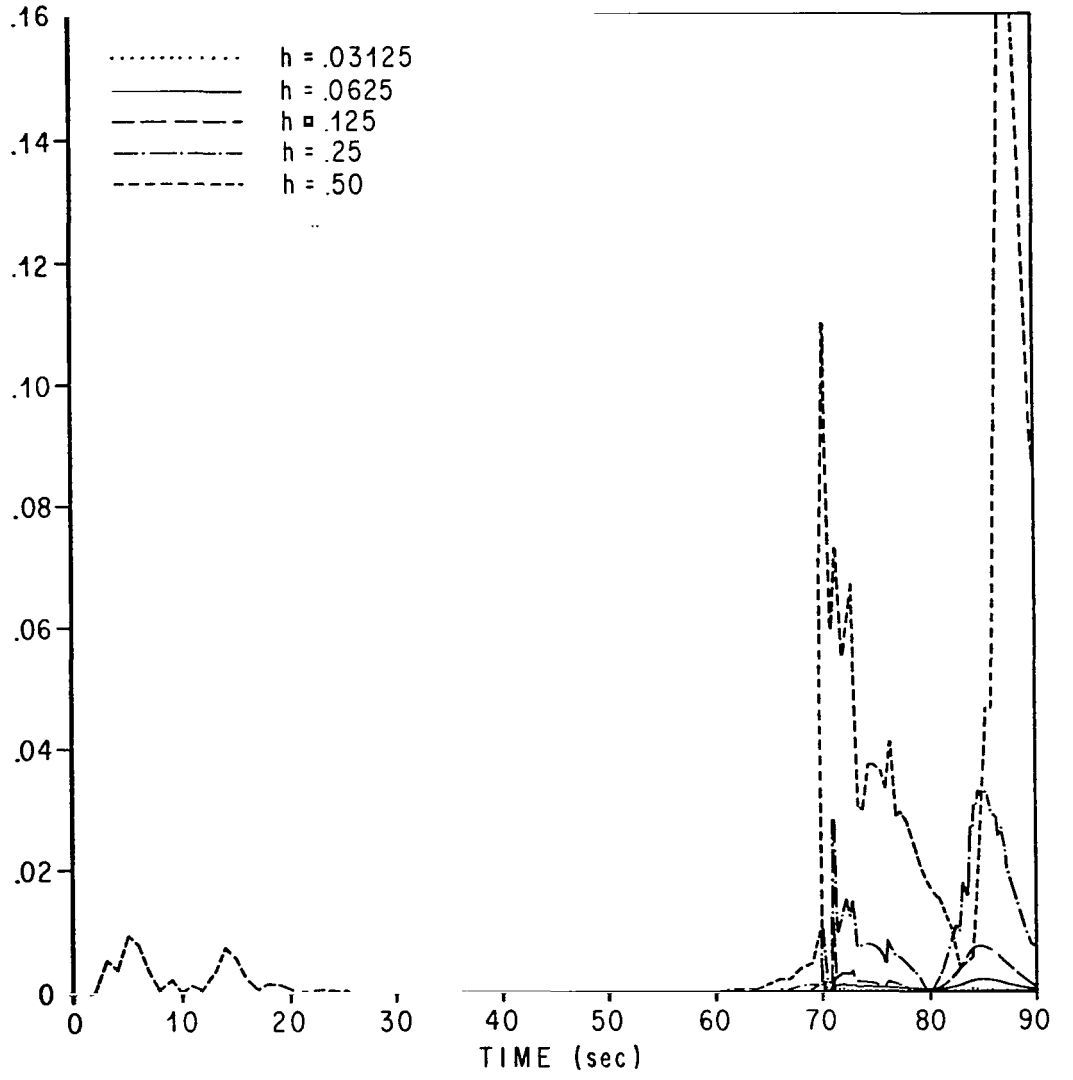

FIG. 23. REGULATOR FOR $\left(\frac{dY_s}{dt}\right) = \int_{t_n}^{t_n+h} \left(\frac{d^2Y_s}{dt^2}\right) dt$

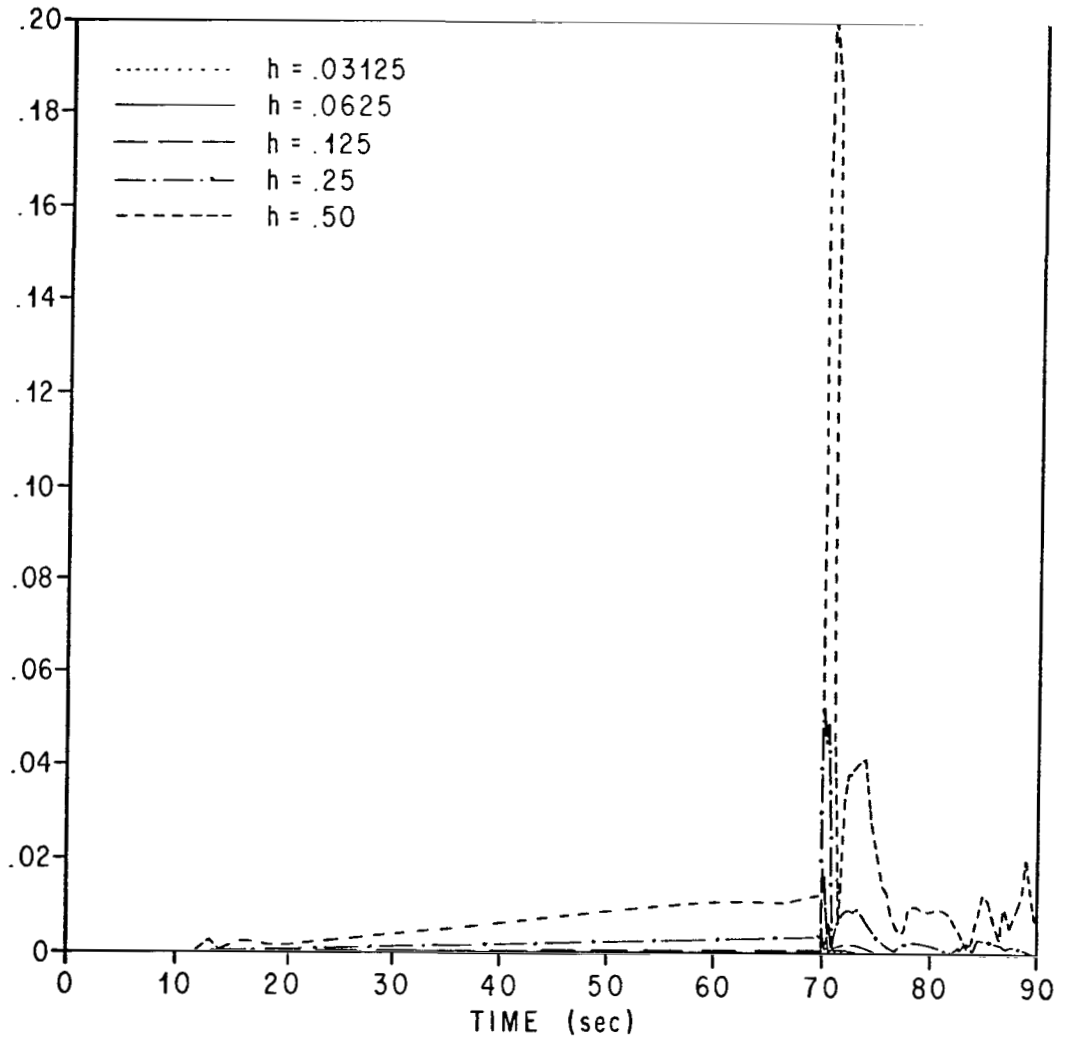

FIG. 24. REGULATOR FOR $\left(\frac{dZ_s}{dt}\right) = \int_{t_n}^{t_n+h} \left(\frac{d^2Z_s}{dt^2}\right) dt$

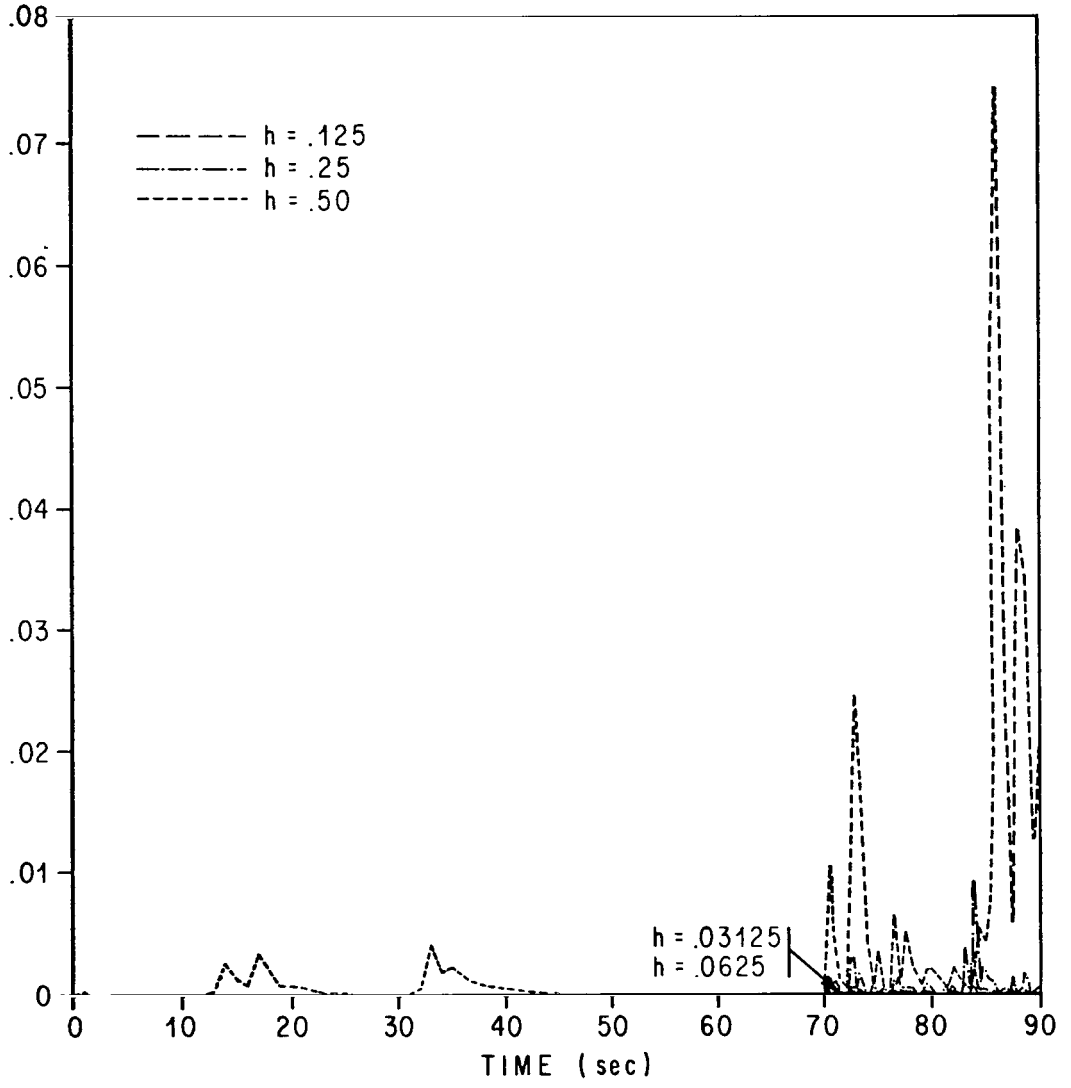

FIG. 25. REGULATOR FOR $\omega_x = \int_{t_n}^{t_n+h} \left(\frac{d\omega_x}{dt}\right) dt$

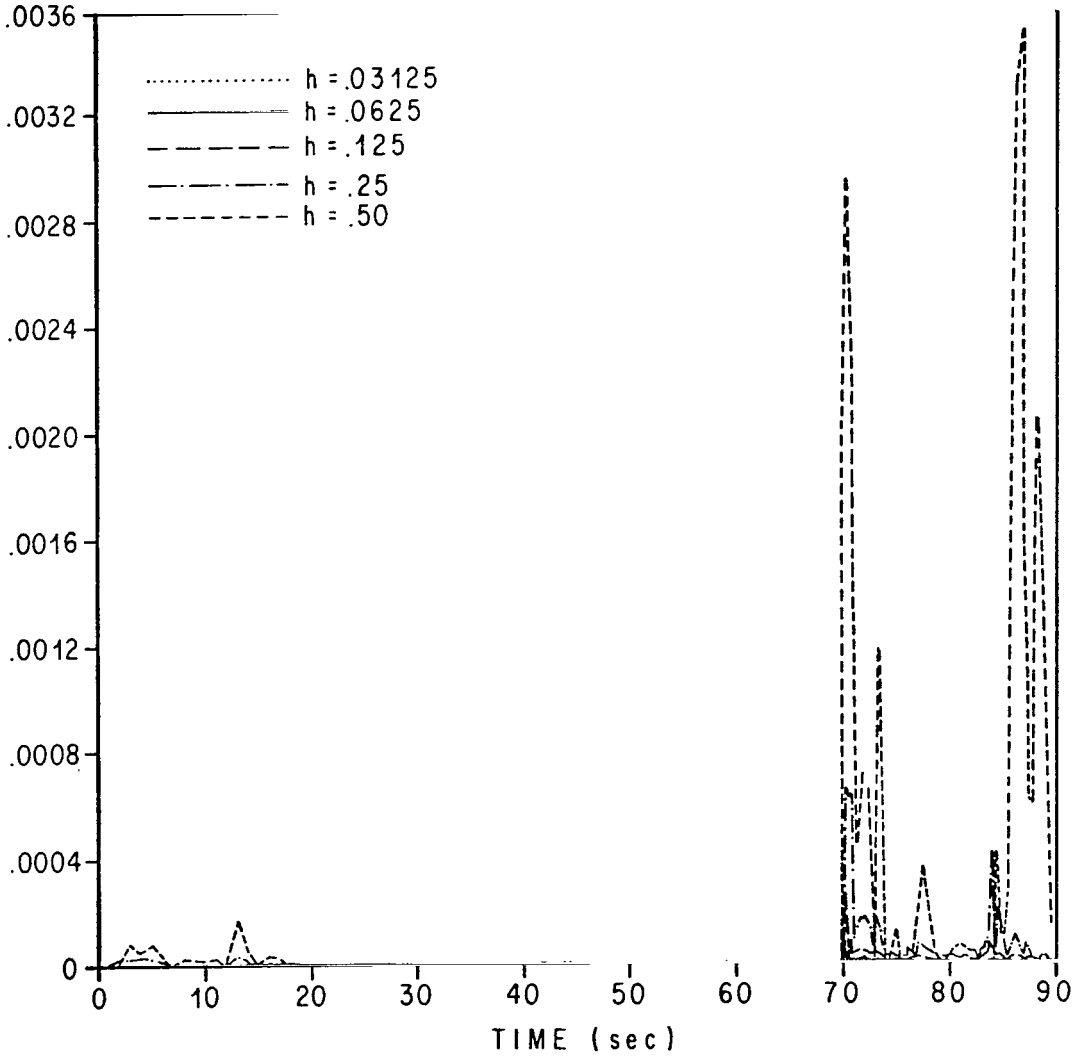

FIG. 26. REGULATOR FOR $\omega_y = \int_{t_n}^{t_n+h} \left(\frac{d\omega_y}{dt}\right) dt$

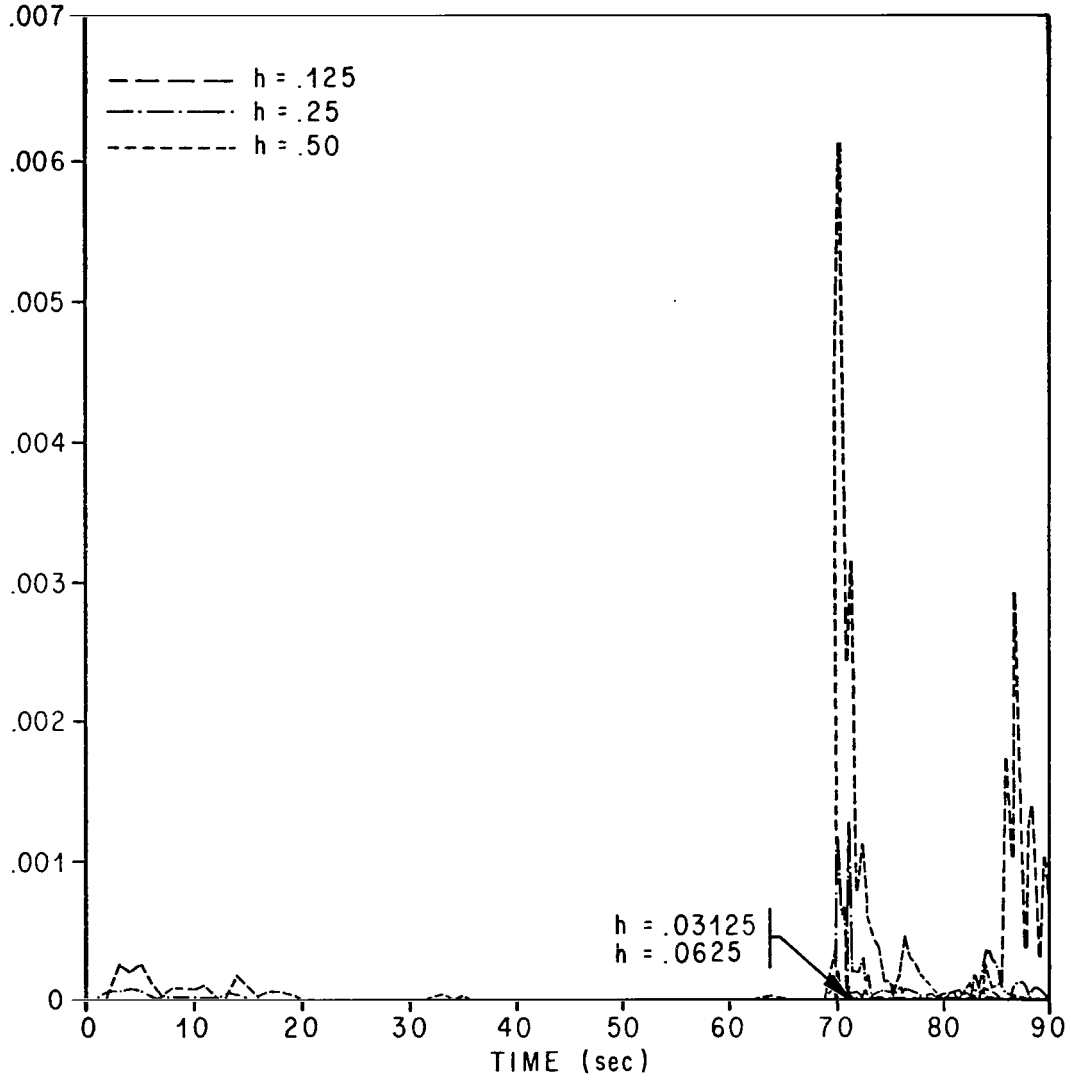

FIG. 27. REGULATOR FOR $\omega_z = \int_{t_n}^{t_n+h} \left(\frac{d\omega_z}{dt}\right) dt$

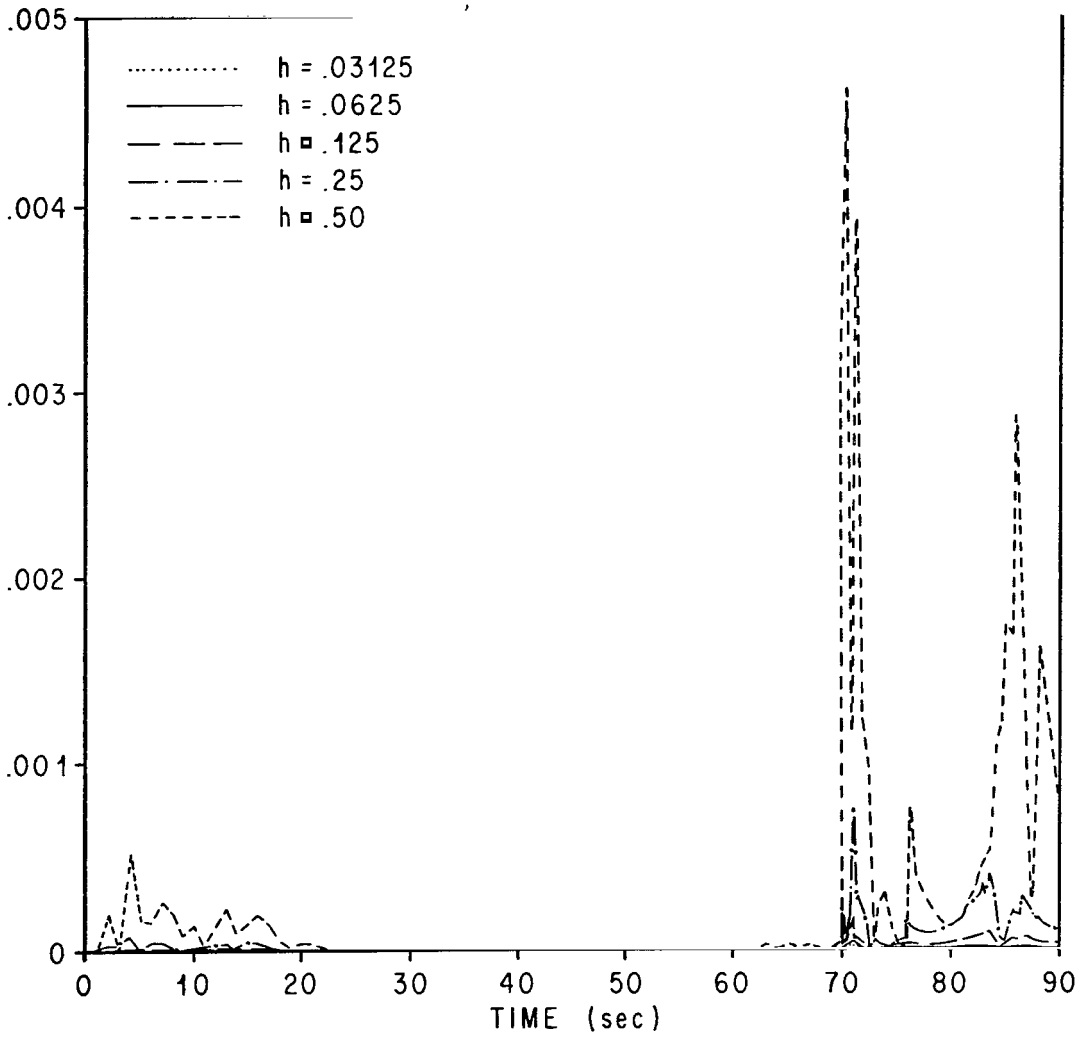

FIG. 28. REGULATOR FOR $\varphi_p = \int_{t_n}^{t_n+h} \left(\frac{d\varphi_p}{dt}\right) dt$

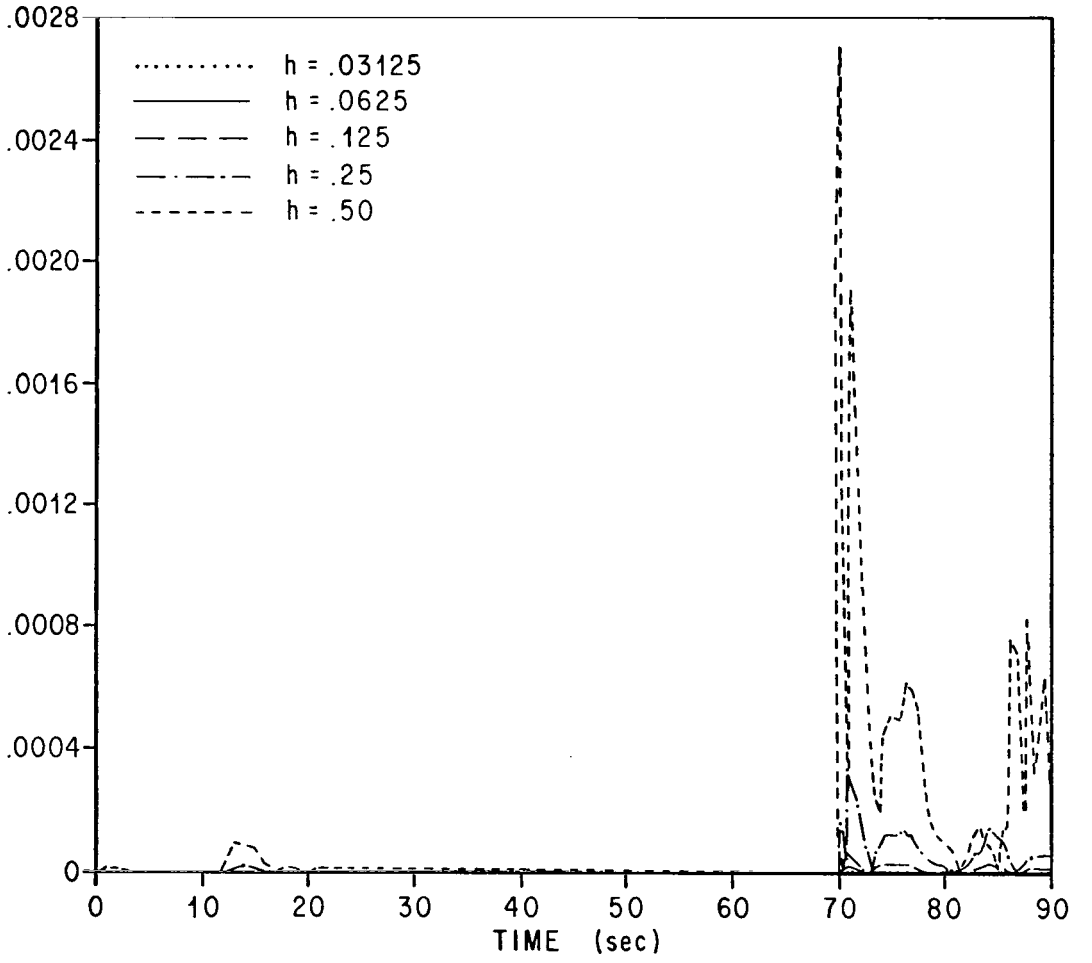

FIG. 29. REGULATOR FOR $\varphi_y = \int_{t_n}^{t_n+h} \left(\frac{d\varphi_y}{dt}\right) dt$

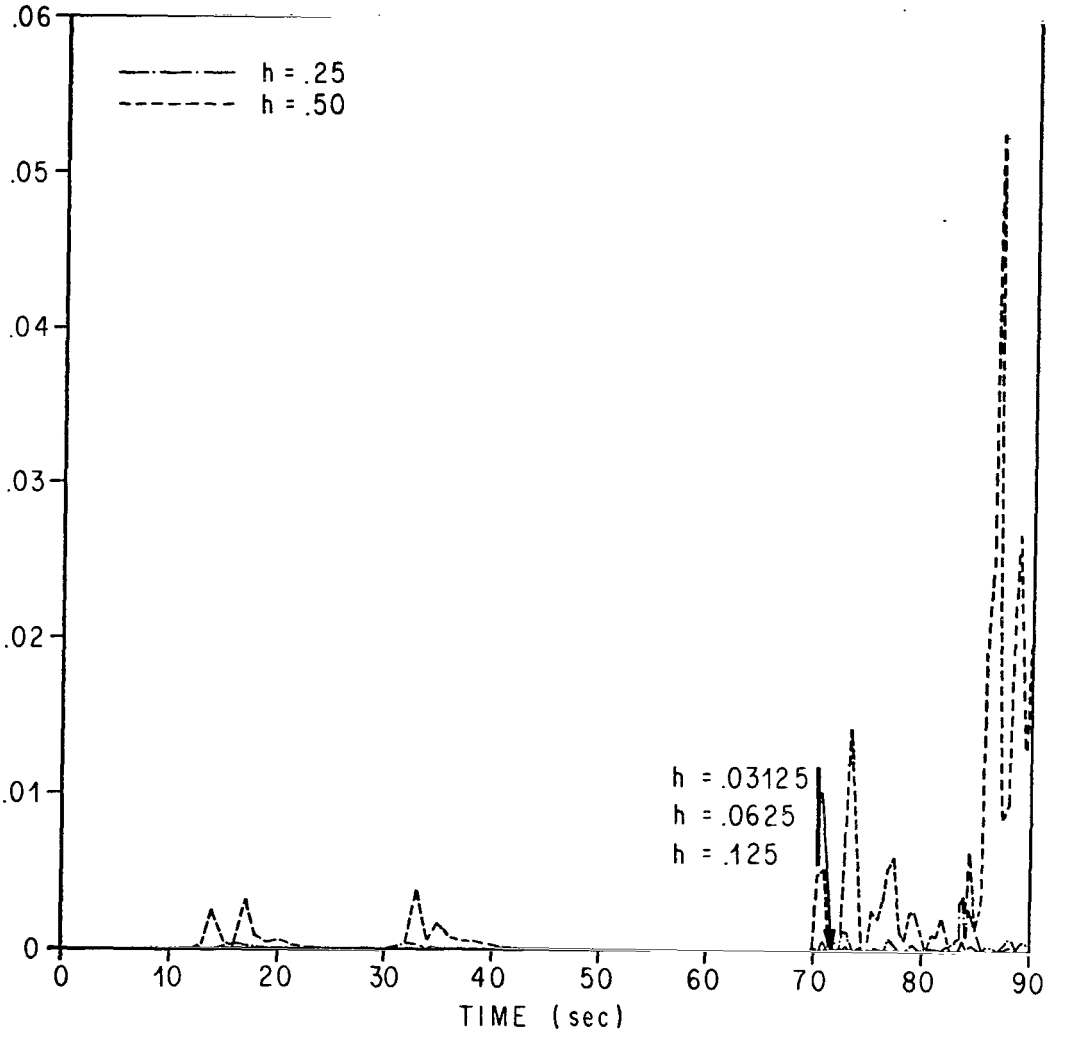

FIG. 30. REGULATOR FOR $\varphi_r = \int_{t_n}^{t_n+h} \left(\frac{d\varphi_r}{dt}\right) dt$

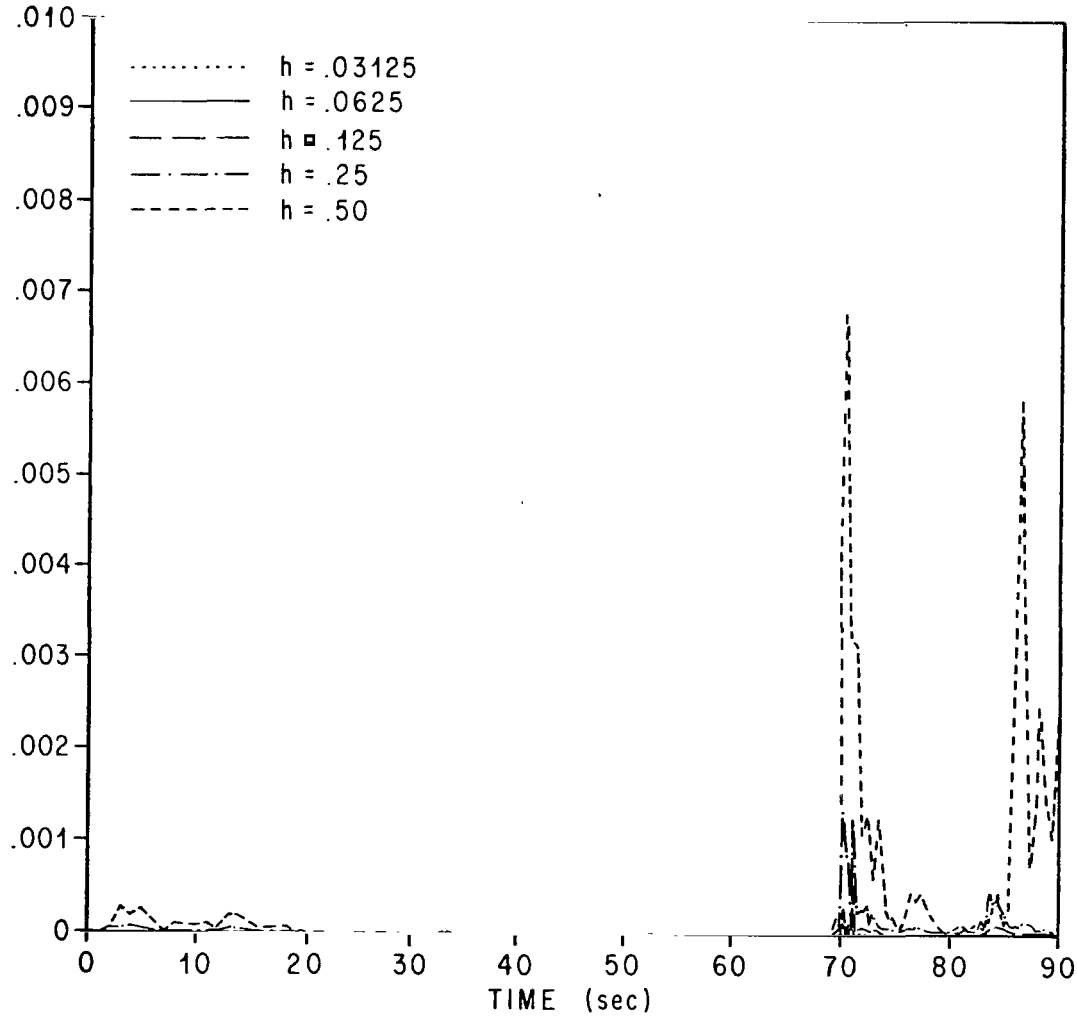

FIG. 31. ROOT-SUM-SQUARE OF REGULATORS FOR INTEGRATING PITCH AND YAW ANGULAR ACCELERATION (FIGURES 26 AND 27)

REFERENCES

1. Heiskanen, W. A., and Moritz, Helmut, Physical Geodesy, Freeman, San Francisco, 1967, Chapters 1 and 2.

2. Smith, O. E., and Weidner, Don K., A Reference Atmosphere for Patrick AFB, Florida, Annual, NASA TMX-53139, 1964.

3. Scheiman, Gerald E., and Brown, Harrold E., A Method to Derive Vehicle Attitude Error Equations, National Aeronautics and Space Administration, IN-R-ASTR-65-12, 1965.

4. Andrus, J. F., Closed Form Solution to Control Equations, National Aeronautics and Space Administration, MTP-COMP-63-2, 1963.

5. Shanks, E. Baylis, New Procedures for Solving Differential Equations, Vanderbilt University Note, August 1968.

6. Shanks, E. Baylis, Higher Order Approximations of Runge-Kutta Type, NASA TN D-2920, September 1965.

7. Shanks, E. Baylis, Error Control for Formulas of Runge-Kutta Type, Vanderbilt University Note, 1968.

8. Shanks, E. Baylis, "Solutions of Differential Equations by Evaluations of Functions," Mathematics of Computation (published by the American Mathematical Society), Vol. 20, No. 93, pp. 21-38, January 1966.

George C. Marshall Space Flight Center
National Aeronautics and Space Administration
Marshall Space Flight Center, Alabama 35812

933-50-00-00-62, August 1, 1969

NASA-Langley, 1969 —— 30

"The aeronautical and space activities of the United States shall be conducted so as to contribute . . . to the expansion of human knowledge of phenomena in the atmosphere and space. The Administration shall provide for the widest practicable and appropriate dissemination of information concerning its activities and the results thereof."

—NATIONAL AERONAUTICS AND SPACE ACT OF 1958

NASA SCIENTIFIC AND TECHNICAL PUBLICATIONS

TECHNICAL REPORTS: Scientific and technical information considered important, complete, and a lasting contribution to existing knowledge.

TECHNICAL NOTES: Information less broad in scope but nevertheless of importance as a contribution to existing knowledge.

TECHNICAL MEMORANDUMS: Information receiving limited distribution because of preliminary data, security classification, or other reasons.

CONTRACTOR REPORTS: Scientific and technical information generated under a NASA contract or grant and considered an important contribution to existing knowledge.

TECHNICAL TRANSLATIONS: Information published in a foreign language considered to merit NASA distribution in English.

SPECIAL PUBLICATIONS: Information derived from or of value to NASA activities. Publications include conference proceedings, monographs, data compilations, handbooks, sourcebooks, and special bibliographies.

TECHNOLOGY UTILIZATION PUBLICATIONS: Information on technology used by NASA that may be of particular interest in commercial and other non-aerospace applications. Publications include Tech Briefs, Technology Utilization Reports and Notes, and Technology Surveys.

Details on the availability of these publications may be obtained from:

SCIENTIFIC AND TECHNICAL INFORMATION DIVISION

NATIONAL AERONAUTICS AND SPACE ADMINISTRATION

Washington, D.C. 20546